

Cool, Luminous, and Highly Variable Stars in the Magellanic Clouds. II: Spectroscopic and Environmental Analysis of Thorne-Żytkow Object and Super-AGB Star Candidates

ANNA J. G. O'GRADY,^{1,2} MARIA R. DROUT,^{1,3} B. M. GAENSLER,^{1,2} C. S. KOCHANEK,^{4,5} KATHRYN F. NEUGENT,^{6,7,2,*}
CAROLYN L. DOHERTY,⁸ JOSHUA S. SPEAGLE (沈佳士),^{1,9,2} B. J. SHAPPEE,¹⁰ MICHAEL RAUCH,³ YLVA GÖTBERG,^{3,*}
BETHANY LUDWIG,^{1,2} AND TODD A. THOMPSON^{4,5}

¹David A. Dunlap Department of Astronomy & Astrophysics, University of Toronto, 50 St. George Street, Toronto, ON, M5S3H4 Canada

²Dunlap Institute for Astronomy & Astrophysics, University of Toronto, 50 St. George Street, Toronto, ON, M5S3H4, Canada

³The Observatories of the Carnegie Institution for Science, 813 Santa Barbara St., Pasadena, CA 91101, USA

⁴Department of Astronomy, The Ohio State University, 140 West 18th Avenue, Columbus, OH 43210, USA

⁵Center for Cosmology and Astroparticle Physics, The Ohio State University, 191 W. Woodruff Avenue, Columbus, OH 43210, USA

⁶Center for Astrophysics — Harvard & Smithsonian, 60 Garden Street, Cambridge, MA 02138-1516, USA

⁷Lowell Observatory, 1400 W Mars Hill Road, Flagstaff, AZ 86001, USA

⁸School of Physics and Astronomy, Monash University, VIC 3800, Australia

⁹Department of Statistical Sciences, University of Toronto, 100 St George Street, Toronto ON, M5S3G3, Canada

¹⁰Institute for Astronomy, University of Hawaii, 2680 Woodlawn Drive, Honolulu, HI 96822, USA

Submitted to The Astrophysical Journal, Jun 10 2022, Accepted Nov 20 2022

ABSTRACT

In previous work we identified a population of 38 cool and luminous variable stars in the Magellanic Clouds and examined 11 in detail in order to classify them as either Thorne-Żytkow Objects (TŻOs, red supergiants with a neutron star cores) or super-AGB stars (the most massive stars that will not undergo core collapse). This population includes HV 2112, a peculiar star previously considered in other works to be either a TŻO or high-mass AGB star. Here we continue this investigation, using the kinematic and radio environments and local star formation history of these stars to place constraints on the age of the progenitor systems and the presence of past supernovae. These stars are not associated with regions of recent star formation, and we find no evidence of past supernovae at their locations. Finally, we also assess the presence of heavy elements and lithium in their spectra compared to red supergiants. We find strong absorption in Li and s-process elements compared to RSGs in most of the sample, consistent with super-AGB nucleosynthesis, while HV 2112 shows additional strong lines associated with TŻO nucleosynthesis. Coupled with our previous mass estimates, the results are consistent with the stars being massive ($\sim 4\text{--}6.5M_{\odot}$) or super-AGB ($\sim 6.5\text{--}12M_{\odot}$) stars in the thermally pulsing phase, providing crucial observations of the transition between low- and high-mass stellar populations. HV 2112 is more ambiguous; it could either be a maximally massive sAGB star, or a TŻO if the minimum mass for stability extends down to $\lesssim 13 M_{\odot}$.

Keywords: massive stars, AGB stars, chemically peculiar stars, lithium stars, spectroscopy, stellar kinematics, magellanic clouds

1. INTRODUCTION

While the late stages of stellar evolution are well constrained for many stars, gaps in our knowledge remain,

particularly concerning the after-effects of binary interaction and the transition point between low- and high-mass stellar evolution. While progress can be made by identifying rare classes of stars at unique stages of stellar evolution, in practice multiple plausible identities can often be ascribed to stars that show unusual properties.

One such example is the peculiar star HV 2112 in the Small Magellanic Cloud (Leavitt 1984; Payne

Corresponding author: Anna O'Grady
anna.ogradey@mail.utoronto.ca

* Hubble Fellow

Gaposchkin & Gaposchkin 1966), with two proposed identities. First, Levesque et al. (2014) classify it as a candidate Thorne-Żytkow Object (TŻO), which is a Red Supergiant (RSG) with a neutron star (NS) core (Thorne & Żytkow 1975, 1977). TŻOs are potential outcomes of binary evolution following the creation of a high mass X-ray binary (HMXB) where, unlike binary neutron star (BNS) progenitors, the common envelope is not ejected. Confirming their existence would place important constraints on the rates of BNS merger events. Second, it could be a massive AGB (mAGB, $M \lesssim 6.5 M_{\odot}$) star (Beasor et al. 2018) or a super-AGB (sAGB, $6.5 \lesssim M \lesssim 12 M_{\odot}$) star (Tout et al. 2014), the latter of which are the most massive stars that will not undergo iron core collapse (Siess 2010; Jones et al. 2013; Doherty et al. 2017). sAGBs bridge the low-mass/high-mass divide, and their exact mass range has crucial consequences on the number of expected core collapse supernovae (CC-SNe) and subsequent chemical enrichment of the universe. Despite representing rare end-states for very different evolutionary pathways, differentiating between sAGBs and TŻOs photometrically or spectroscopically is difficult.

In O'Grady et al. (2020, hereafter Paper I) we tackled this by establishing that there exists a broader class of stars in the Small and Large Magellanic Clouds (SMC; LMC) with photometric and variability properties similar to HV 2112. While originally identified as having stronger than expected Li and heavy element absorption (see below), HV 2112 is also distinguished in being luminous, very cool, and showing very high amplitude variability with a peculiar double-peak morphology. We identified 10 additional stars¹ (collectively dubbed 'HV 2112-like-objects' or HLOs) which all have surface temperatures $T < 4800\text{K}$, luminosities $\log(L/L_{\odot}) > 4.3$, variability periods $P > 400$ days, variability amplitudes $\Delta V > 2.5$ mag, and a double peak feature in their light curves. We also identify 27 additional stars (dubbed 'High Amplitude Variables' or HAVs) that lack the double-peaked light curve but may still belong to the same overall class. Summary tables for the HLOs and HAVs are available in Tables 2 and C1 in Paper I, respectively.

In Paper I we used the physical and variability properties and total population numbers to assess the nature of the HLO/HAVs. Broadly, they have infrared colors sim-

ilar to oxygen-rich AGB stars, do not display signs of enhanced mass loss, are not consistent with observed RSG behavior, and have inferred lifetimes of a few $\times 10^4$ years. Their temperatures and luminosities place them in the region of the Hertzsprung-Russel diagram expected for massive and super-AGB stars, though TŻO stars may also fall in this range. Critically, we combined their pulsation periods and measured radii with MESA stellar evolution (version 10398, Paxton et al. 2011, 2015, 2018, 2019) and GYRE stellar pulsation (Townsend & Teitler 2013) models to estimate current masses for these stars of $\sim 5\text{--}14 M_{\odot}$. Details of the models are provided in §5.2.1 and §5.4 in Paper I. This is *smaller* than the theoretical minimum mass for stable TŻOs of $M_{\min} \sim 15 M_{\odot}$ (Cannon 1993; Podsiadlowski et al. 1995), but consistent with the expected range for massive and superAGB stars, with most of the HLOs tending towards higher masses.

Thus, in Paper I we favored a sAGB star identity for these stars, including HV 2112, in large part because of the mass diagnostic. However, this property is uncertain. Modern sAGB models include many advances made in stellar evolution theory over the past decades, while no modern TŻO models exist. Thus, assumptions had to be made about the internal structure of TŻOs in order to estimate their masses. While a shift in mass large enough to elevate all the HLOs above $15 M_{\odot}$ would require far larger uncertainties on our constrained physical properties than observed, the mass range for HV 2112 in particular was estimated to be $7.5\text{--}14 M_{\odot}$, just under M_{\min} . Therefore a TŻO identity is still possible should the mass be underestimated. In addition, the theoretical M_{\min} is strongly dependent on the treatment of the mass of the NS, mixing length theory, and convection in the models, and thus the true minimum mass for TŻOs may be lower than $15 M_{\odot}$, as discussed in detail in §7.2.4 in Paper I. (Cannon 1993). In that case, mass alone would not be sufficient to distinguish a TŻO from the most massive sAGB stars.

To this end, we expand our analyses to further test the true identity of these stars. Here we analyze the local kinematics, local star formation history, radio environment, and (for a subset of stars) spectroscopy of the HLO/HAV sample. Motivation for each are explained in the following paragraphs, and each section will explain the relevant expectations for TŻOs and sAGBs given the available models. Collectively, these analyses will further elucidate the true nature of these stars.

Kinematic Environment (§2): As the formation of a TŻO requires a supernova explosion, that explosion may impart a recoil velocity to the resulting TŻO. In order for the NS to merge with the secondary, the binary must

¹ 11 stars were initially identified in Paper I, but one (LMC-2) was found in that study to have physical properties consistent with a RSG. It is not included in this present paper, but the naming conventions of the HLOs remains consistent with Paper I, thus the label LMC-2 is skipped.

remain bound, which can lead to a wide range of runaway or smaller ‘walkaway’ velocities (van den Heuvel et al. 2000; Eldridge et al. 2011; Renzo et al. 2019). We will compare the proper motions of the HLOs and HAVs to their local environments to determine if any of the sample possess kinematic properties suggestive of a supernova origin.

Local Star Formation History (§3): We will compare the local star-formation histories (SFHs) of the HLOs/HAVs using detailed maps of the star formation history of the Magellanic Clouds (Harris & Zaritsky 2004, 2009) to those of younger (RSGs/HMXBs) and older populations (AGBs). Since TŻO progenitors are stars with $M \geq 15M_{\odot}$, and given the short ($\sim 10^5 - 10^6$ yr) lifetime of the TŻO phase (Cannon 1993; Biehle 1994), we expect TŻOs to be associated with areas of more recent ($\sim 1 \times 10^7$ yr) star formation. For sAGB stars, the total pre-AGB lifetime is predicted to be $\sim 2-6 \times 10^7$ yrs (Doherty et al. 2017).

Radio Environments (§4): We may expect to see a supernova remnant (SNR) at the location of a TŻO candidate. We will use the large number of radio surveys of the Clouds available to search the locations of the HLOs/HAVs for evidence of SNRs, or of a wind-driven bubble blown by the TŻO progenitor system within which a SNR could be expanding (Ciotti & D’Ercole 1989). We do not expect evidence of SNRs around sAGB stars, though the most massive sAGBs could have blown a wind-bubble while on the main sequence.

Spectroscopy (§5): Both TŻOs and sAGB stars are expected to be enhanced in lithium (Cameron 1955; Cameron & Fowler 1971) and heavy elements (Cannon 1993; Biehle 1994; Podsiadlowski et al. 1995; Lau et al. 2011; Karakas & Lattanzio 2014). Indeed, HV 2112 was first identified as a TŻO candidate by Levesque et al. (2014) who reported strong absorption in Li, Rb, and Mo compared to RSGs (although Beasor et al. 2018, when comparing to stars of similar spectral type, found only a possible Li enrichment). While the nucleosynthetic process in TŻO and sAGB stars lead to similar abundance patterns, subtle differences in both heavy element abundance patterns as well as the relative timing of Li and heavy element enhancement can lead to discernible differences. We use high resolution spectroscopy to search for any excess of heavy elements in our population.

Finally, the combined results of these analyses are discussed in §6.

2. LOCAL KINEMATICS

Here we analyze the astrometry of the HLOs and HAVs relative to their local environments. If these stars

are TŻOs, we might expect to find evidence of a previous supernova in their kinematic properties (Thorne & Żytkow 1975; Leonard et al. 1994). As radial velocities are not available for many of the stars, we instead focus on proper motions from *Gaia* Early Data Release 3 (EDR3, Gaia Collaboration et al. 2020) to assess 2D plane-of-sky velocities.

2.1. Kinematic Expectations

The peculiar velocity expected for a TŻO system depends on its formation channel. However, with the exception of dynamical formation in a dense stellar cluster, all channels require a relatively tight binary that both remains bound and has a secondary mass $>15 M_{\odot}$ after the primary explodes to form a NS. In such systems, the runaway velocity is primarily the recoil induced by the mass lost during the supernova. The impact of a random kick imparted to the NS is small, as this impulse is distributed over the (large) mass remaining in the system (Liu et al. 2015). For TŻOs formed from high-mass X-ray binaries that subsequently undergo common envelope evolution (Taam et al. 1978) recoil velocities range from $\sim 10-80$ km s^{-1} with higher mass systems falling on the upper end of this range (van den Heuvel et al. 2000). For TŻOs that instead form when the natal kick leads to an eccentric NS orbit with a pericenter distance inside the radius of the secondary, the median expected runaway velocity is ~ 75 km s^{-1} (Leonard et al. 1994).

With distances of 62.1 ± 1.0 kpc (Graczyk et al. 2014) and 50.0 ± 1.3 kpc (Pietrzyński et al. 2013) a velocity of 80 km s^{-1} would correspond to a proper motion of 0.27 and 0.34 mas yr^{-1} in the SMC and LMC, respectively. The kinematics of the Magellanic Clouds in the *Gaia* data have been studied extensively (e.g., Gaia Collaboration et al. 2018a, 2020; Lennon et al. 2018; Oey et al. 2018; Dorigo Jones et al. 2020) and local trends in proper motion due to, for example, the rotation of the galaxies are evident down to levels of $\lesssim 0.1$ mas yr^{-1} . Thus, depending on location with the Clouds, the higher runaway velocities predicted for TŻOs may be detectable relative to the local background stars if oriented in the plane of the sky. On the other hand, we do not expect sAGBs to have significantly different kinematics from the other stars in their local environments. The non-detection of a significant peculiar velocity would be agnostic between these two origins.

2.2. Selection and Properties of Local Comparison Samples

We obtain astrometric measurements from *Gaia* EDR3. For each HLO and HAV, we select all *Gaia* sources within 5 arcminutes of the star with *Gaia* $G <$

18 mag. This corresponds to a physical scale of ~ 70 and ~ 90 pc in the LMC and SMC, respectively, chosen to be significantly smaller than the physical scale over which trends due to the galaxy rotation are evident (Gaia Collaboration et al. 2018b).

2.2.1. Removal of Foreground Sources

To avoid contamination from foreground sources in our comparison sample, we follow a procedure similar to that outlined in Paper I, based on the methods of Gaia Collaboration et al. (2018b). First, we remove all sources with parallax over parallax error (π/σ_π) > 4 . Then, we compare the kinematic properties of the remaining stars to the 2D distribution of proper motions formed by a sample of $\sim 1,000,000$ highly probable LMC/SMC members (see Paper I for details). We assume our distribution of proper motions can be modeled as a two-dimensional Gaussian with some unknown mean $\vec{\mu} = (\bar{\mu}_\alpha, \bar{\mu}_\delta)$ and covariance matrix $\mathbf{C} = \begin{bmatrix} c_{\alpha\alpha} & c_{\alpha\delta} \\ c_{\delta\alpha} & c_{\delta\delta} \end{bmatrix}$.

After accounting for the individual measurement uncertainties $\sigma_{\alpha,i}$ and $\sigma_{\delta,i}$ from each object i , the total likelihood across all objects becomes

$$\ln L = -\frac{1}{2} \sum_i (\vec{\mu}_i - \vec{\mu})^T (\mathbf{C}_{\text{tot},i})^{-1} (\vec{\mu}_i - \vec{\mu}) + \ln(\det(2\pi\mathbf{C}_{\text{tot},i})) \quad (1)$$

where $\vec{\mu}_i = (\mu_{\alpha,i}, \mu_{\delta,i})$ is the proper motion of object i , $\mathbf{C}_{\text{tot},i} = \mathbf{C} + \begin{bmatrix} \sigma_{\alpha,i}^2 & 0 \\ 0 & \sigma_{\delta,i}^2 \end{bmatrix}$ is the effective ‘‘total’’ covariance for object i , T is the transpose operator, and \det is the determinant.

Since larger measurement uncertainties lead to larger covariances, this approach naturally weights the contribution of individual objects based on their overall measurement uncertainties. We use `scipy.optimize.minimize` to minimize the total negative log-likelihood in order to determine the optimal 5-parameter solution. We will denote this estimated optimal mean and covariance as $\vec{\mu}_*$ and \mathbf{C}_* , respectively, to avoid confusion with the true unknown mean and covariance $\vec{\mu}$ and \mathbf{C} .

For each star j in each region, we then calculate a chi-square statistic as $\chi_j^2 = (\vec{\mu}_j - \vec{\mu}_{\text{med}})^T \mathbf{C}_*^{-1} (\vec{\mu}_j - \vec{\mu}_{\text{med}})$, where $\vec{\mu}_j$ is the proper motion of star j , $\vec{\mu}_{\text{med}}$ is the median proper motion of the comparison sample, and \mathbf{C}_* is again the optimal covariance matrix derived earlier. Sources that fall outside the region containing 99.5% of highly probable LMC/SMC members, corresponding to $\chi^2 > 10.6$, are removed as likely foreground stars. An average of 6.4% of stars in each HLO or HAV region are removed.

2.2.2. Kinematic Properties of the Local Environments

The local comparison sample for each HLO/HAV contains approximately 500 stars. In Figure 1, we plot μ_α and μ_δ for the stars surrounding the 10 HLOs, after subtracting off the center-of-mass proper motions for the LMC/SMC². The weighted mean and standard deviations for the stars in each of these regions, indicated by a grey cross in Figure 1, are also listed in Table 1. The fields have residual mean proper motions, relative to the center-of-mass of the Clouds, ranging from ~ 0.0 – 0.3 mas yr⁻¹, and standard deviations of ~ 0.1 – 0.15 mas yr⁻¹ (corresponding to velocity dispersions of ~ 25 – 45 km s⁻¹ in the LMC and SMC).

2.3. Comparison of HLO/HAV Kinematics to their Local Environments

The EDR3 proper motions for the 10 HLOs are given in Table 1 and plotted in Figure 1. None of the HLOs fall completely outside of the distribution of local stars, though several (e.g. SMC-2, SMC-6) lie near the edge. Here we quantitatively assess the location of the HLOs/HAVs within 2D distribution of proper motions, and place constraints on any peculiar velocity exhibited by the stars.

All of the HLOs and HAVs have a positive and significant Gaia EDR3 ‘excess noise’ parameter (ϵ_i), which is a measure of how discrepant the astrometric solution of a source is from the expected model. It is expected to be close to zero for good fits. A significant excess noise could be due to instrumental errors, or intrinsic effects that affect the location of the photocenter such as binarity (Lindgren et al. 2012, 2018). It has also been suggested that single-star variability may lead to increased excess noise (Gandhi et al. 2020). We additionally assess the impact of this through the 1D distribution of total proper motions in Appendix A.

2.3.1. Location within the 2D Distribution of Local Proper Motions

We calculate the χ^2 statistic of each HLO and HAV compared to the 2D distribution of the proper motions of nearby stars. We follow the same procedure described above for the removal of foreground sources, but this time optimizing the covariance matrix using the ~ 500 stars in each region, excluding the HLO/HAV itself. The resulting χ^2 statistic encodes what fraction of the local stars have kinematics that lie interior to that of the HLO/HAV. In Table 1 we report the χ^2 values and cumulative distribution function (CDF) percentage of each HLO or HAV.

² $(\mu_\alpha, \mu_\delta) = (1.89, 0.31)$ and $(0.69, -1.23)$ mas/yr for the LMC and SMC, respectively (Gaia Collaboration et al. 2018b).

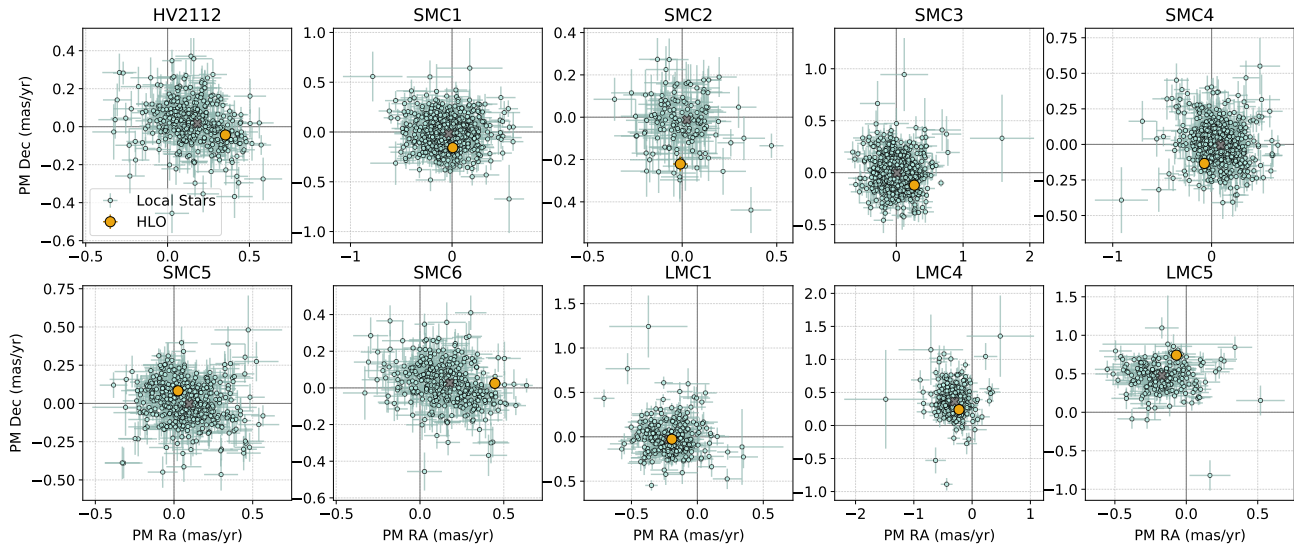


Figure 1. The proper motions of the HLOs (in gold) and all stars within 5 arc minutes that are likely Magellanic Cloud stars (in pale blue). A dark grey cross indicates the weighted mean proper motion for each group of stars. The median proper motion of the Clouds have been subtracted.

None of the HLOs or HAVs fall outside the kinematic region defined by 99% of the stars in their local environments, consistent with inspecting Figure 1. However, 5 HLOs (50%) and 9 HAVs (33%) do lie in the outer 25% of their local distributions. To assess the significance of this, we performed an additional analysis on the 1-D distributions of total proper motions of the HLOs/HAVs. Compared to 5000 other Magellanic Cloud stars with similar levels of astrometric excess noise as the HLOs/HAVs, we see similar results. Thus, we do not see evidence that the HLOs have unusual total proper motions relative to their local mean given (i) the local dispersions and (ii) their astrometric excess noise, likely induced by their strong variability. The details of this assessment are provided in Appendix A.

2.3.2. Limits on Peculiar Tangential Velocity

Here, we calculate the total tangential velocity of the HLOs/HAVs relative to the local mean. We convert the total residual proper motions to velocities. The results are listed in Table 1 and shown on the right axes of Figure A1. When calculating the errors listed in Table 1, we consider both the statistical errors on measurements of proper motion in RA and Dec from *Gaia* and the systematic uncertainty in distance due to the line-of-sight depth of the stellar distribution of the LMC and SMC (5.0 and 10.0 kpc, respectively; Yanchulova Merica-Jones et al. 2017), though the Cloud depths did not contribute significantly to the final uncertainty.

The HLOs exhibit tangential velocities relative to their local means of 5–83 km s⁻¹, with over half falling below 50 km s⁻¹. Results are similar for the HAVs.

While a peculiar velocity >30 km s⁻¹ is typically considered the criterion for classification as a “runaway” star (Blaauw 1961), given (i) the velocity dispersions of ~ 40 km s⁻¹ in the region around each HLO/HAV and (ii) our finding above that the residual proper motions of the HLO/HAVs are consistent with expectations for a random sample of stars with similar astrometric excess noise, we consider these velocities *limits* on the tangential component of any kick imparted to the systems during an earlier phase in their evolution. In conclusion, while we do not find evidence for large (and significant) peculiar velocities, given the range of predictions for TZOs outlined in § 2.1, this is not particularly constraining on the origin of the systems.

3. LOCAL STAR FORMATION HISTORIES

Here, we assess the relative ages of the stellar populations surrounding the HLOs/HAVs. As TZOs and sAGB stars form from different mass progenitor stars, their average local SFH should differ. We use the Harris & Zaritsky (Harris & Zaritsky 2004, 2009, HZ hereafter) SFH maps of the LMC/SMC. Constructed using photometry of millions of individual stars from the Magellanic Cloud Photometric Survey (Zaritsky et al. 2002, 2004), the HZ maps present SFHs in grids of 12'x12' boxes, corresponding to 175x175 and 200x200 pc in the LMC and SMC, respectively. Star formation rates within each box are presented as a function of look-back time (ranging from 4 Myr to 10 Gyr) and divided into three metallicity bins. Previous studies have used these maps to constrain the ages of populations of stars and supernova remnants (Badenes et al. 2009; Williams et al. 2018; Auchetti et al.

Table 1. Kinematic properties of the HLOs.

HLO	μ_α^a	μ_δ^a	$\mu_{\alpha,loc}^b$	$\mu_{\delta,loc}^b$	χ^2	CDF ^c	μ^d	CDF ^c	Velocity ^e	σ_{Local}^f
	(mas/yr)	(mas/yr)	(mas/yr)	(mas/yr)			2D			
HV 2112	0.35 ± 0.04	-0.04 ± 0.03	0.18 ± 0.15	0.02 ± 0.09	1.65	56.2%	0.18 ± 0.03	56.0%	53 ± 13	30
SMC-1	0.01 ± 0.04	-0.16 ± 0.03	-0.03 ± 0.14	-0.02 ± 0.11	1.60	55.0%	0.14 ± 0.03	43.2%	43 ± 12	39
SMC-2	-0.01 ± 0.04	-0.22 ± 0.03	0.03 ± 0.10	-0.01 ± 0.09	8.08	98.2%	0.21 ± 0.03	76.1%	62 ± 15	27
SMC-3	0.27 ± 0.05	-0.12 ± 0.04	0.01 ± 0.16	0.00 ± 0.11	3.05	78.1%	0.28 ± 0.05	78.3%	83 ± 20	42
SMC-4	-0.07 ± 0.05	-0.13 ± 0.04	0.09 ± 0.14	-0.01 ± 0.10	3.58	83.3%	0.21 ± 0.04	67.1%	62 ± 17	38
SMC-5	0.03 ± 0.03	0.08 ± 0.03	0.10 ± 0.15	0.00 ± 0.11	0.59	25.5%	0.11 ± 0.03	28.0%	33 ± 11	32
SMC-6	0.45 ± 0.04	0.02 ± 0.03	0.18 ± 0.15	0.03 ± 0.10	4.21	87.8%	0.27 ± 0.04	82.8%	79 ± 17	30
LMC-1	-0.19 ± 0.04	-0.03 ± 0.04	-0.22 ± 0.11	-0.03 ± 0.13	0.01	0.5%	0.02 ± 0.04	2.0%	5 ± 9	34
LMC-4	-0.22 ± 0.04	0.24 ± 0.04	-0.30 ± 0.12	0.36 ± 0.14	0.92	36.8%	0.14 ± 0.04	41.3%	34 ± 10	41
LMC-5	-0.07 ± 0.04	0.74 ± 0.05	-0.17 ± 0.14	0.48 ± 0.17	4.38	88.8%	0.28 ± 0.05	75.9%	67 ± 15	36

^aWith the proper motion of the SMC (0.685, −1.230) and LMC (1.890, 0.314) mas/yr (Gaia Collaboration et al. 2018a) subtracted

^bThe mean weighted proper motion and standard deviation of the likely Cloud members in the 5′ circle around the associated HLO. Cloud proper motion has been subtracted.

^cCumulative density function. The percentage denotes how much of the distribution is interior to that HLO.

^dThe proper motion of the Cloud and the mean weighted proper motion of the local environment (columns 4 and 5) have been subtracted.

^eSpeed relative to the average speed of stars in the local environment. Error includes proper motion measurement error, distance measurement error, and error due to Cloud depth.

^fStandard deviation of the proper motion of stars in the 5 arcmin bubble around each HLO.

2019; Sarbadhicary et al. 2021; Díaz-Rodríguez et al. 2021).

3.1. Star Formation History Expectations

Expectations for SFHs in the local environments surrounding TŻOs and sAGB stars depend on a combination of properties intrinsic to the stellar systems (e.g. progenitor mass, lifetime, natal kick) and details of the measurement methodology (e.g. physical and temporal resolution). Although the initial mass range that leads to sAGB stars is thought to be about 2–3 M_\odot wide, due to its dependence on factors such as metallicity, convective overshooting, and rotation, the initial stellar mass range that may produce sAGB stars can range from ~ 6.5 –12 M_\odot (García-Berro & Iben 1994; Poelarends et al. 2008; Doherty et al. 2017). The total pre-AGB lifetime is $\log(t_{\text{years}}) \sim 7.5 - 7.8$ (Doherty et al. 2017). No kick is expected in the prior evolution of sAGB stars, and hence they should remain in their birth environment.

For TŻOs, the primary of the binary system must be massive enough to explode and form a NS, and the secondary must have a mass $M_{\text{min}} \geq 15 M_\odot$ at the time of the supernova, with the caveat that M_{min} may be lower, as discussed in §1. Together these constrain the

mass of the primary to be ~ 12 –30 M_\odot , with the lower masses only possible for low mass ratio binaries where the secondary accretes mass during Case B mass transfer (e.g., van den Heuvel et al. 2000). The subsequent delay-time between the supernova explosion and TŻO formation is expected to be small: negligible for TŻOs formed via a NS kick and $\lesssim 10^5$ years for TŻOs formed from high mass X-ray binaries that enter a common envelope phase (Podsiadlowski et al. 1995). Similarly, while the TŻO lifetime is uncertain, current estimates range from $\sim 10^4$ – 10^6 years (Cannon 1993; Biehle 1994; Tout et al. 2014). Thus, the age of a TŻO system should be dominated by the lifetime of the primary star, and range from $\log(t_{\text{years}}) \sim 6.7 - 7.2$.

While a velocity will be imparted to a TŻO system by the supernova, the short delay-time and lifetime limit the distance it can travel from its birth environment. Even with the maximal peculiar velocity of $\lesssim 80 \text{ km s}^{-1}$ found in § 2, a system would travel $\lesssim 80 \text{ pc}$ in 10^6 years—still within a single cell in the HZ star formation history maps. Thus, we may expect that a population of TŻOs would be associated with areas of more recent star formation, compared to a population of sAGBs. The key to the analysis is only in part the association of the HLOs

with specific HZ age bins. It is also how the clustering of the HLOs in age compares to the clustering of other stellar populations with well understood physical properties – these differences and similarities should hold independent of any shortcomings of the HZ star formation histories. We assess this using samples of comparison stars, below.

3.2. Method Description

We use the HZ SFH maps to assess the ages of the stellar populations that produce the HLOs/HAVs *relative to those that produce other classes of stars* (e.g. RSGs, AGBs). We use the approach of Kochanek (2022), which is based in turn on those of Badenes et al. (2009, 2015). Here, we review key aspects of this methodology.

We first combine the HZ metallicity bins into a single star formation history $s_i(j)$ for each spatial bin indexed by j and age indexed by i . The SFH maps for the LMC and SMC used different temporal bins, so we need to analyze them separately, though we reduce the overall number by 2 by combining adjacent temporal bins. If the “efficiency” with which a population of stars is produced at a given age is ϵ_i , then the expected number of stars associated with spatial bin j is

$$e_j = \sum_i \epsilon_i s_i(j). \quad (2)$$

If the actual number of stars in a spatial bin is n_j , the Poisson likelihood of the distribution is

$$\ln L = \sum_{stars} \ln \left(\frac{r e_j^{n_j}}{n_j!} \right) - \sum_{all} r e_j, \quad (3)$$

where the first sum is over the spatial bins containing stars and the second sum is over all bins. We can discard the factorial $n_j!$ since it is just a constant contribution to the likelihood.

If we maximize Eqn. 3 for the efficiencies ϵ_i , the uncertainties will include the Poisson uncertainties in the number of stars. However, what we require is the maximum likelihood solution for how to distribute a fixed number of stars over the age bins. We do this by introducing the “renormalization factor” r into Eqn. 3. Optimizing the likelihood with respect to the renormalization factor, we find that

$$r = N \left[\sum_{all} e_j \right]^{-1}, \quad (4)$$

where $N = \sum n_j$ is the total number of stars. We then renormalize $\epsilon_i \rightarrow r \epsilon_i$, which also rescales $e_j \rightarrow r e_j$ so that $\sum e_j = N$. Effectively, we have converted the Pois-

son likelihood into the multinomial likelihood for the distribution of the N stars over the age bins.

Operationally, we are using Bayesian statistics with the likelihoods and uncertainties determined using Markov Chain Monte Carlo (MCMC) methods, with $\log e_j$ as the variables. For each trial, the values of the ϵ_i are renormalized before evaluating the likelihood. To avoid having some $\log e_j \rightarrow -\infty$ we included a weak prior, further discussed in Kochanek (2022), of

$$\lambda^{-2} \sum_i \left[\ln \left(\frac{\epsilon_i \Delta t_{i+1}}{\epsilon_{i+1} \Delta t_i} \right) \right]^2, \quad (5)$$

on adjacent temporal bins with $\lambda = 6.91$ in the likelihood. This is purely to avoid numerical problems and has no significant effect on the results. The number of stars formed per unit SFR is $\propto \epsilon_i \Delta t_i$ where Δt_i is the temporal width of the bin, so the prior adds a penalty of unity to the likelihood if adjacent bins differ in the number of stars produced per unit SFR by a factor of 1000. The prior is just to ensure numerical stability and has no significant impact on the results. We note that this analysis does not require that a given target population is complete, but does assume that the completeness does not vary across spatial bins. This should be true for the HLO/HAV populations.

If all objects in a target population were formed at a single time in the past, then one would nominally expect the number of objects associated with that time bin to equal the total number in the population and the number of objects associated with every other temporal bin to be zero. However, since the SFHs in each spatial bin are not fully orthogonal, some spillover to other temporal bins is expected in this analysis—*especially when the population being examined has a small number of objects*.

To assess this, if we create fake stellar samples associated with particular age bins and distribute them following the HZ star formation histories, the method always identifies the correct age bin, in the sense that the distribution peaks in the correct bin. As an empirical test, we divided the OGLE IV Magellanic Cloud fundamental mode Cepheid samples (Soszyński et al. 2015, 2016, 2017) into four logarithmic periods bins and used these methods to estimate their ages. Shorter periods correspond to lower masses and hence longer main sequence lifetimes, where we used the relationships between age, mass and period from Anderson et al. (2016). As seen in Figure B2 in Appendix B, the four period bins largely sort themselves in the correct age order except for the longest periods, where there are also very limited numbers of Cepheids.

The covariances in the SFR in this type of analysis are very strong. Therefore the published uncertainties, which are simply the diagonal elements of the matrix and not the full covariances, are not directly useful for these calculations. This is why we focus much of the discussion on comparisons between well defined stellar populations, as these differences should be little affected by the unmodelled covariances. The above tests demonstrate that this method is capable of qualitatively distinguishing between populations over the age ranges expected for TŻO and sAGB stars (Section 3.1).

Thus we perform a qualitative comparison of the predicted ages of the HLOs and HAVs *relative to a well-chosen set of comparison samples* rather than performing a detailed quantitative assessment of the resulting age distributions directly.

3.3. Comparison Sample Selection

To assess the relative ages of the stellar populations in the regions surrounding the 7(3) HLOs and 3(16) high-luminosity HAVs in the SMC(LMC), we examined four comparison populations for each galaxy:

- *Red Supergiants* – With estimated initial masses between ~ 14 – $25 M_{\odot}$ these RSGs should have similar ages to TŻOs. Sample Size: 28 in SMC, 104 in LMC.
- *High Mass X-Ray Binaries* – HMXBs with periods shorter than 100 days are predicted to be the direct ($\lesssim 10^5$ year delay-time) precursors to TŻOs in one of the main formation channels (Taam et al. 1978). Sample Size: 38 in SMC, 10 in LMC.
- *High-luminosity oxygen-rich AGB stars* – With absolute K_s mag < -8.95 , this is expected to probe masses $\gtrsim 5 M_{\odot}$, indicative of massive or super AGB stars. Sample Size: 46 in SMC, 169 in LMC.
- *Low-luminosity oxygen-rich AGB stars* – With expected ages older than either TŻO or sAGB stars, this sample provides a long-baseline control. Sample Size: 344 in SMC, 2258 in LMC.

The RSGs are from the catalogs of Massey & Olsen (2003), Yang & Jiang (2011, 2012), and Davies et al. (2018). From Levesque et al. (2005) we calculate rough masses for 123 of these 132 RSGs using the relationship $\log(M/M_{\odot}) = 0.5 - 0.1M_{bol}$, which is based on fitting the Geneva evolutionary models to the mid-point of the RSG branch. Using $M_{bol} = -2.5 \times \log L_{\odot} + 4.75$ we adopt luminosities from Neugent et al. (2020); Massey et al. (2021). Based on this approximate relationship,

the RSGs in our comparison sample range from ~ 14 – $25 M_{\odot}$, with a majority between 15 – $20 M_{\odot}$. This is similar to the mass range expected for TŻOs, and indicates that our sample is not dominated by either very high or low mass RSGs.

The HMXBs come from the catalogs of Haberl & Sturm (2016) and Antoniou & Zezas (2016) for the SMC and LMC, respectively. While only $\sim 30\%$ of HMXBs in the Clouds have measured orbital periods, the sample with known periods is not expected to be spatially biased.

Finally, the AGBs are from Boyer et al. (2011, 2015). We use only AGB stars that fall in the “oxygen-rich” branch, because the HLOs fall on the high-luminosity end of this sequence in the infrared color-magnitude diagram (see Paper I). For our divide between our high- and low-luminosity comparison samples, we take the $K_s = 9.6$ magnitude of LMC-3, one of the stars originally identified in Paper I, with an estimated mass of ~ 2 – $4 M_{\odot}$ based on its pulsation properties as the dividing point. It should therefore roughly separate higher mass AGB stars ($M \geq 5 M_{\odot}$; $\log(t) \lesssim 8.3$) from from lower mass systems ($M \leq 4 M_{\odot}$; $\log(t) \sim 9.0$).

3.4. Results: HLOs Relative to Other Populations

Figure 2 shows the fraction of each population that is associated with each age bin. We do not show the bin by bin uncertainties in Figure 2 for the reasons outlined in §3.2. We do give in Table C1 (Appendix C) the log likelihoods for the HLOs or HLOs+HAV populations to have the same age distribution as each of the comparison populations. These likelihoods take full account of the covariances up to the limitation discussed in §3.2 that we lack the covariance information for the ZH SFR histories.

In the top panels of Figure 2 we see that the RSGs (red) are associated with young age bins. This effect is particularly strong in the LMC where the RSGs are concentrated in the youngest age bin, while in the SMC there is some blurring of the population out to $\log(t_{\text{years}}) \sim 8.0$. However, in both galaxies the RSGs are clearly associated with younger populations than the AGB stars. HMXBs (pink) are also associated with young populations, and are the population most similar to the RSGs, as expected. In both galaxies we then observe the expected progression: high-luminosity AGBs (dark blue) are associated with older populations than RSGs/HMXBs and low-luminosity AGBs (light blue) are associated with older populations than high-luminosity AGBs. We note that some contamination between the observed samples of RSGs and high-

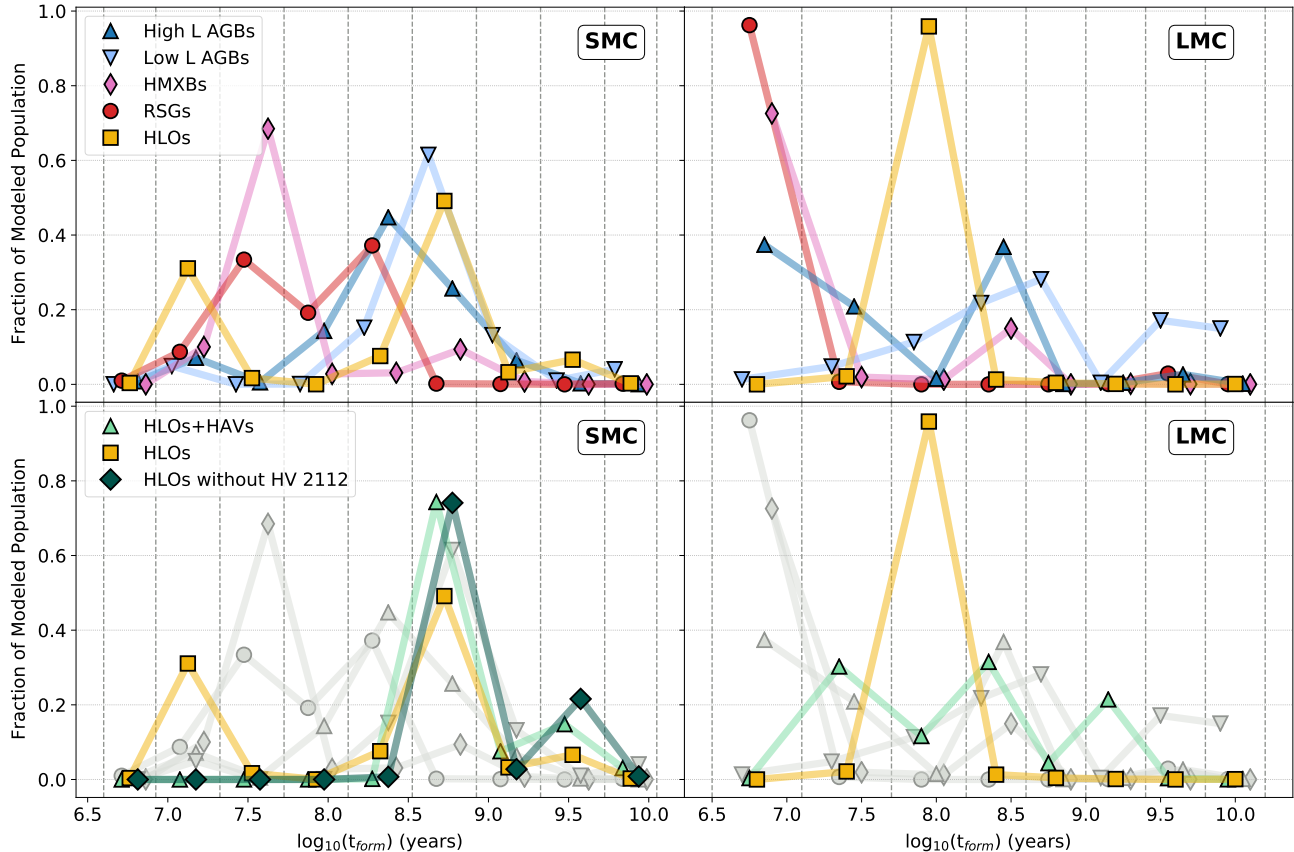


Figure 2. *Top:* The fraction of each stellar population in the SMC (left) and LMC (right) located within each HZ age bin. The edges of the age bins are marked by vertical dashed lines. The HLOs are in gold, high-luminosity AGBs in dark blue, low-luminosity AGBs in light blue (see §3.3 for the distinction), RSGs in red, and HMXBs in pink. The HLOs are centered in the bins, with other populations slightly offset to aid in viewing. Uncertainties are not shown (see §3.2) *Bottom:* The same as above, but with the combined population of HLOs and high luminosity HAVs as light green triangles, the population of HLOs without HV 2112 as dark green diamonds, and other populations greyed out.

luminosity AGBs may exist, but this should not radically change the results.

The population of HLOs is shown in gold. In the LMC (right panels), the HLOs clearly peak at formation times older than RSGs/HMXBs and slightly younger than AGB populations. The SMC the population appears to have two peaks, one younger at earlier formation times than RSG/HMXB populations, and one older, stronger peak which is more closely associated with AGB populations. This bimodal nature of the SMC HLOs is not as conclusive as the LMC population. However, upon examining the star formation histories in the regions around the stars, we found that the region containing HV 2112 has a strong peak in star formation around $\log(t_{\text{years}}) \sim 7.0$. If we remove HV 2112 from the SMC HLO population and repeat the analysis (dark green, bottom right panel of Figure 2), the younger peak disappears and the rest of the sample strongly favours ages more similar to AGB stars.

In the bottom panels of Figure 2, we also show the results for the combined sample of HAVs and HLOs. In the SMC, the combined population matches the distributions of the HLOs without HV 2112 closely. In the LMC, where the population increases from 3 HLOs to 19 HLOs+HAVs, the distribution widens, but broadly peaks in the same area at the HLO population and not in the youngest bin with the RSG/HMXB populations.

If these stars were TZOs, we might expect them to be consistently associated with regions of the most recent star formation, similar to their progenitor HMXBs. Thus, except for HV 2112, the SFH of the HLO/HAV population is better aligned with a sAGB star origin.

4. RADIO ENVIRONMENT

Here we search for evidence of previous supernova explosions at the locations of the HLOs and HAVs by searching for extended radio structures using the wealth of available data for the Magellanic Clouds.

4.1. Radio Environment Expectations

The birth of a TŻO requires the death of a massive star in a SN explosion, leaving behind a SNR. In the Magellanic Clouds, SNRs have been found in surveys across a range of frequencies (Mathewson & Clarke 1973; Filipović et al. 2005; Williams et al. 1999; van der Heyden et al. 2004). Observable SNRs in the MCs have a range of physical sizes up to a cutoff at 30 pc in radius (Badenes et al. 2010). This corresponds to an angular size of 1.6 arcmin in the SMC and 2.1 arcmin in the LMC. Assuming a typical SNR fading time of $\sim 6 \times 10^4$ yr (Frail et al. 1994; Maoz & Badenes 2010), the SNR could be visible early in the TŻO lifetime of $\sim 10^5 - 10^6$ yr (Cannon 1993; Biehle 1994). We have no reason to think that the selection of the HLOs and HAVs in Paper I was biased against younger TŻOs, though the lack of a SNR would not be conclusive evidence against a TŻO identity. Alternatively, the massive O-type binary progenitor system of a TŻO may have blown a wind bubble in the ISM. While the SNR would then not be visible until it traverses the low density medium inside the bubble, the bubble itself could be visible as an expanding shell in radio observations (Ciotti & D'Ercole 1989).

Should our stars truly be sAGBs, we would not expect to see any SNRs. The most massive sAGBs ($\sim 12M_{\odot}$) may have had strong enough winds during the main sequence lifetime to blow a wind bubble, potentially visible as a HI shell (Gervais & St-Louis 1999; Cappa & Herbstmeier 2000; Gaensler et al. 2005).

4.2. Data

Here we summarize the radio data we consider:

Continuum Maps: The spatial resolution for each map is indicated in parentheses, along with the equivalent distance in parsecs. For the SMC we use ATCA continuum images at 2.37 (0'67/12pc), 4.80 (0'58/11pc), and 8.64 (0'37/7pc) GHz (Filipović et al. 2002), and ASKAP continuum images at 960 (0'5/9pc) and 1320 (0'27x0'25/5pc) MHz (Joseph et al. 2019). In the LMC we use ATCA continuum images at 4.80 (0'49/9pc) and 8.64 (0'37/5pc) GHz (Dickel et al. 2005), and ASKAP continuum images at 887 (0'23x0'20/3pc) MHz (Harvey-Smith et al. 2016). We note that SNRs have been discovered and analyzed in all of these maps (Filipović et al. 2005; Bozzetto et al. 2014; Joseph et al. 2019).

HI Velocity Cubes: HI cubes for the SMC were taken with ASKAP (DeBoer et al. 2009; McClure-Griffiths et al. 2018), with a spectral resolution of 4 km/s and a spatial resolution of 0'58x0'45 (~ 9 pc at the distance of the SMC). The LMC HI data were taken with ATCA (Kim et al. 2003), with a spectral resolution of 1.7 km/s

and spatial resolution of 1' (~ 15 pc at the distance of the SMC/LMC).

4.3. Supernova Remnants & Other Extended Structures

Searching catalogs of SNRs in the Magellanic Clouds (Badenes et al. 2010; Bozzetto et al. 2017; Maggi et al. 2016, 2019), we find none at the locations of the HLOs or HAVs.

In the various continuum maps described in §4.2, we see no bubbles or other structures at the locations of any of the HLOs (except HV 2112, see §4.4) and HAVs. For all but the archetypal HLO HV 2112, we see no evidence of any expanding shells, nor any other coherent structure, within the HI velocity cube. In the highest resolution ASKAP map, the mean $3\text{-}\sigma$ upper limit on the surface brightness at the location of the star assuming a radius of 30 pc (Badenes et al. 2010) in the SMC is $\Sigma_{1\text{GHz}} < 0.5 \text{ W m}^{-2} \text{ Hz}^{-1} \text{ sr}^{-1}$, and in the LMC is $\Sigma_{1\text{GHz}} < 1.1 \text{ W m}^{-2} \text{ Hz}^{-1} \text{ sr}^{-1}$. In Appendix D we show the surface brightness upper limit at 30 pc for all HLOs and HAVs in Table D2. While we cannot rule out the existence of a very faint ($\Sigma_{1\text{GHz}} < 10^{-22} \text{ W m}^{-2} \text{ Hz}^{-1} \text{ sr}^{-1}$) SNR at the location of any of the stars, there is no evidence of any visible SNR for the HLOs or the HAVs.

The expected number of SNR is $N_{\text{SNR}} = n_{\text{obj}} \frac{t_{\text{SNR}}}{t_{\text{TZO}}}$ where n_{obj} is 11 (HLOs) or 38 (HLOs+HAVs), t_{SNR} is the fade time of 6×10^4 yr, and t_{TZO} is 10^5 - 10^6 yr. The probability of having no SNRs, $e^{-N_{\text{SNR}}}$, ranges from 0.1-51% for HLOs only and ~ 0 -10% for HLOs+HAVs. Unless we assume that HLOs and HAVs are separate populations (unlikely, from Paper I) and take the longest possible TŻO lifetime, the chance of observing no SNRs if these stars are TŻOs is small.

4.4. HV 2112 Structure

The only structure of note within the HI data at the location of any of the HLOs is a U-shaped structure surrounding HV 2112 – the TŻO candidate that defines the properties used to select the other sources – at an LSR velocity of 116.8 km/s. The structure is shown in the top right panel of Figure 3. It has a radius $R \sim 27$ pc (the radius of a circle that best fit the three sides of the U shape), an approximate projected area of 1890 pc², and a mean brightness temperature (background subtracted) of 36 ± 3 K. We do not see evidence of an expanding structure in the RA vs V and Dec vs V images, shown in the top left and bottom right panels of Figure 3. We therefore assume an upper limit on the expansion velocity of $v_{\text{exp}} \sim 4$ km/s, the channel width. This is less than the velocity of typical random

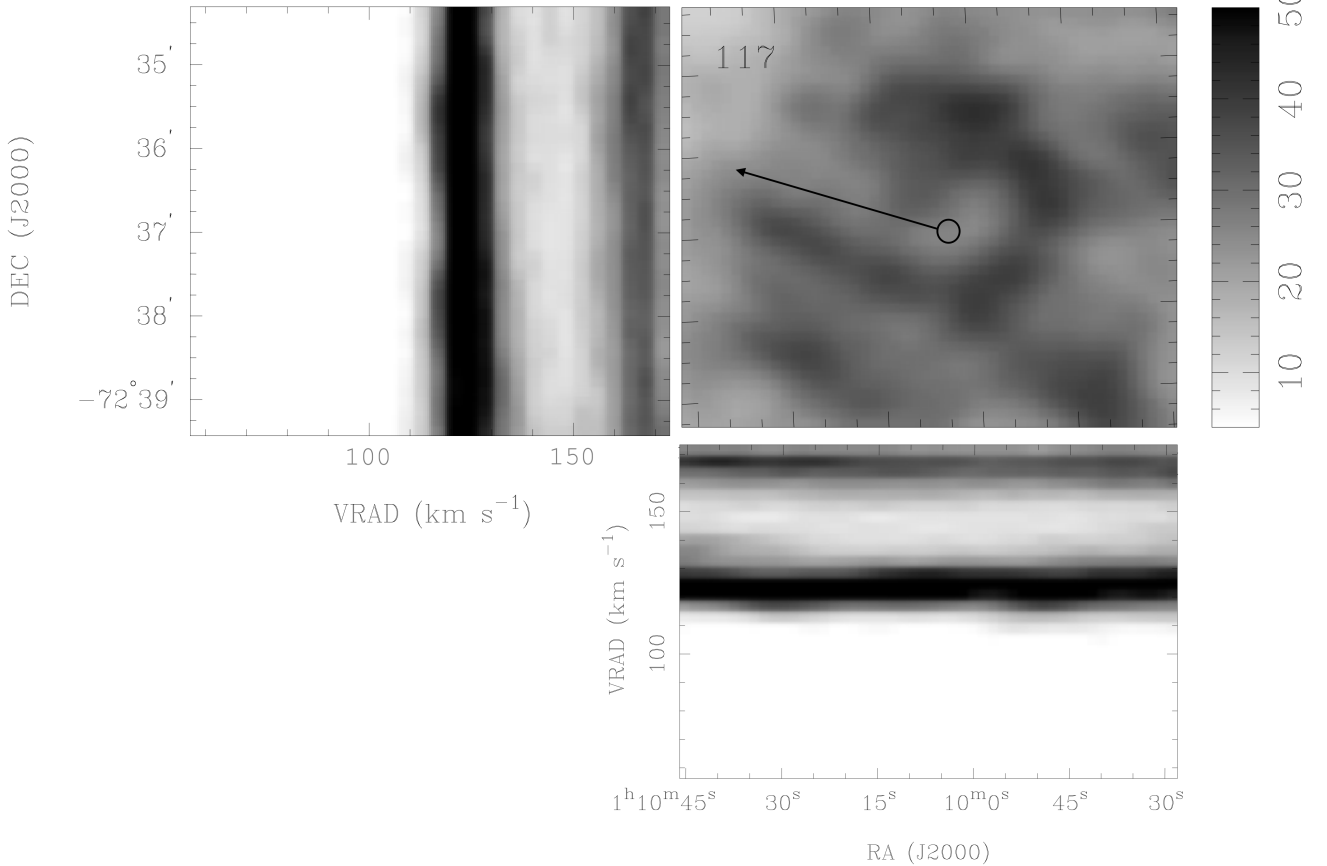


Figure 3. HI cube from ASKAP data at the location of HV 2112. The panels show the brightness temperature in RA vs DEC at an LSR velocity of 117 km/s (top right), RA vs LSR velocity at a DEC of $-72:36:54$ (top left), and LSR velocity vs DEC at an RA of 01:10:04. The spatial resolution of the data is $0.5'$ and the velocity resolution is 4 km/s. The position of HV 2112 in RA vs DEC is shown with a circle, and the direction of proper motion of HV 2112 (minus the motion of the SMC) is indicated with an arrow. At a velocity of ~ 53 km/s (Table 1), HV 2112 would take ~ 1 Myr to travel the length of the arrow.

ISM motions, so if it is not a random fluctuation, it must be a short lived structure. The HI column density through the structure is $(7 \pm 2) \times 10^{19} \text{ cm}^{-2}$. If spread throughout a sphere of radius 27 pc, the average pre-existing ambient number density is $n_o \approx 0.5 \pm 0.2 \text{ cm}^{-3}$, or $\rho_o \approx 8 \pm 3 \times 10^{-25} \text{ g cm}^{-3}$. In the interior of the structure, the mean brightness temperature is 18 ± 1 K, which gives $n_{o,int} = 0.02 \pm 0.01 \text{ cm}^{-3}$.

We follow the same steps as Gaensler et al. (2005) to investigate the possible identity of this structure.

4.4.1. Random ISM fluctuation

The maximum expansion velocity of $v_{exp} \leq 4$ km/s is on the order of random fluctuations in the ISM (~ 10 km/s for an ISM temperature of ~ 8000 K). It is therefore entirely possible that this structure is a transient, random feature in the ISM and not related to HV 2112.

4.4.2. Supernova Remnant

Sedov-Taylor Adiabatic Expansion: If this structure is a SNR in the Sedov-Taylor phase (where no heat is

exchanged with the surrounding ISM), the radius and velocity are $R_{ST} = 1.54 \times 10^{19} (E_{51}/n_o)^{1/5} t_3^{2/5} \text{ cm}$ and $V_{ST} = 1950 (E_{51}/n_o)^{1/5} t_3^{-3/5} \text{ km/s}$ where $E_{51} = E/10^{51}$ ergs and $t_3 = t/10^3$ yr (Draine 2011). Using these equations to eliminate the age t we find an explosion energy $E \sim 2.5 \pm 1.3 \times 10^{46}$ ergs, far less than the 10^{51} ergs expected for a SN. Thus this structure cannot be the Sedov-Taylor phase of a SN energy explosion.

Radiative or Snowplow Phase: If the structure is a SNR in the radiative phase (where momentum is constant), we must first find the time and radius at which the SNR left the Sedov-Taylor phase and transitioned to the radiative phase. Assuming $E = 10^{51}$ ergs and using $t_{tran} = 49.3 \times 10^3 E_{51}^{0.22} n_o^{-0.55} \text{ yr}$ and $R_{tran} = 7.32 \times 10^{19} E_{51}^{0.29} n_o^{-0.42} \text{ cm}$, we find $t_{tran} = 7 \pm 2 \times 10^4$ yr and $R_{tran} = 32 \pm 5$ pc. The observed radius of $R = 27$ pc falls within this range. In the radiative phase, $R_{Rad} = R_{tran} (t/t_{tran})^{2/7}$ and $V_{Rad} = (2/7) R_{Rad}/t$ (Draine 2011). For $R_{Rad} = 27$ pc, we should see $V_{Rad} = 180 \pm 120$ km/s. We see no evidence of an expanding

bubble within this velocity range in the HI data. We therefore conclude that the structure is not a SNR.

4.4.3. Current Wind Bubble

In order to determine if the structure could be a current wind bubble, we calculate the wind power and associated mass loss rate required to blow a bubble with $R = 27$ pc for a wind with luminosity L_w expanding into a medium of density ρ_o . We use $R = 0.76(L_w/\rho_o)^{1/5}t^{3/5}$ and $v_{exp} = R/t$ (Weaver et al. 1977). With a maximum v_{exp} of 4 km/s, we find a minimum age of $t = 4.0 \pm 0.2$ Myr and maximum central stellar wind power of $L_w = (7 \pm 4) \times 10^{33}$ ergs/s. The wind power is related to the mass loss rate \dot{M} and wind speed by $L_w = \frac{1}{2}\dot{M}v_w^2$ (Weaver et al. 1977). In Paper I we found that HV 2112 had to have a $\dot{M} < 3.8_{-0.5}^{+0.9} \times 10^{-7} M_\odot/\text{yr}$. For this \dot{M} the wind velocity would need to be $v_w = 240_{-60}^{+70}$ km/s. This is significantly higher than observed for AGB stars (5-15 km/s, Höfner & Olofsson 2018). RSGs typically have slightly higher wind velocities (~ 30 km/s, van Loon et al. 2005), and TŻOs are assumed to have wind speeds similar to RSGs (Cannon 1993; Biehle 1994). Additionally, if the structure was related to the current wind of HV 2112, we might expect the U shape to be a bow-shock related to the motion of HV 2112. However, the proper motion of HV 2112, indicated in Figure 3 with an arrow, is pointing away from the bright emission arc. Thus this structure cannot be related to the current mass loss rate of HV 2112, whether it is a super-AGB star or TŻO.

4.4.4. Old Wind Bubble

Two possibilities remain, both relating to a bubble driven by a wind from a previous stage of HV 2112's evolution. If the bubble was driven by a previous wind, the current maximum expansion velocity of ≤ 4 km/s could be slower than the original expansion of the wind-driven bubble.

sAGB identity: First, if HV 2112 is a super-AGB star with a mass of $\sim 8-14 M_\odot$ (estimated in Paper I), its main sequence progenitor would be an early type B star. Assuming values of $\dot{M} = 1.6 \times 10^{-9} M_\odot/\text{yr}$ and $v_\infty = 4380$ km/s for a $M=12.7M_\odot$ B1V star (Krtićka 2014), and therefore a wind power of $L_w = 9.7 \times 10^{33}$ erg/s, a wind-driven bubble with the ambient density and current radius would be 3.6 ± 0.6 Myr old and have an expansion velocity of 4.5 ± 0.7 km/s. This expansion velocity could be consistent with this structure, though we note again that we cannot observationally constrain whether the bubble is truly expanding. For a sAGB star in the mass range of $6-12M_\odot$, the time since the main sequence phase (consisting mostly of the core He burning phase) would be $\sim 2-4$ Myr (Doherty et al. 2017).

Thus this structure may be a wind-blown bubble from the main sequence progenitor of a super-AGB star.

TŻO identity: The picture is more complex if HV 2112 is a TŻO. One of the progenitor components of the TŻO system must be a star with $M > 15 M_\odot$, and the other must be $\sim 12-30 M_\odot$ (see §3.1). Both stars would have strong, line-driven winds on the main sequence, and could form a bubble. The later supernova would therefore not be observable as an SNR as it travels through the low density ($n_{o,int} \approx 0.02 \text{ cm}^{-3}$) interior of the bubble (Ciotti & D'Ercole 1989). Taking two O9.5V stars with $M = 16 M_\odot$, $\dot{M} = 1.6 \times 10^{-8} M_\odot/\text{yr}$ and $v_\infty = 6700$ km/s (Muijres et al. 2012), we simply sum their wind luminosities to obtain the total L_w for the bubble (Chu et al. 1995; McClure-Griffiths et al. 2001; Benaglia et al. 2005; Ramírez-Ballinas et al. 2019). This gives lower limits on a total wind power of $L_w = 4.5 \times 10^{35}$ erg/s, a minimum age of 1.0 ± 0.2 Myr, and a minimum current expansion velocity of 16 ± 2 km/s. This age is within the predicted lifetime of a TŻO ($\sim 10^5 - 10^6$ yr Cannon 1993; Biehle 1994). However, this expansion velocity should be observable in the ASKAP HI data, and our maximum observed velocity is ~ 4 km/s. This suggests that this structure is not the product of the main sequence winds of a TŻO progenitor system.

4.4.5. Structure Identity Conclusion

To summarize, the most likely identities of the structure around HV 2112 is i) a random fluctuation of the ISM, or ii) a wind-driven bubble produced by the main sequence progenitor of a super-AGB star. The structure is not a supernova remnant, and could not have been created by a TŻO progenitor system.

5. SPECTROSCOPY

Both TŻOs and m/sAGB stars are expected to synthesize high abundances of lithium and an array of heavy elements. In §5.1 we explain in detail the expectations for each class. We present our general procedure in §5.2 and data and reduction techniques in §5.3. Abundance estimates for cool, inflated, stars are complex and model dependent. We use a methodology similar to Levesque et al. (2014), explained in §5.5-5.6, where we assess the presence of potential element enhancements by comparing the ratios of absorption line equivalent widths to the same lines in a population of RSGs of similar temperatures and luminosities. Our results are reported in §5.7. In §5.7.2-5.7.3 we compare our results for HV 2112 to that of Levesque et al. (2014) and Beasor et al. (2018), before finally interpreting the results for the entire population (§5.8).

5.1. Spectroscopic Expectations

5.1.1. TŻO Spectra Expectations

Here we review the predictions for the primary nucleosynthetic outputs, although we must bear in mind that the TŻO models have not been updated in the decades since their introduction, and many theoretical predictions for the observed spectra of TŻOs were developed before several important advances in stellar evolution codes.

The luminosity of supergiant TŻOs comes predominantly from nuclear reactions in the hot atmosphere of the neutron star. To maintain a sufficient temperature for fusion, a minimum envelope mass of $\sim 14M_{\odot}$ and therefore a minimum total mass of $\sim 15M_{\odot}$ is required (Cannon 1993; Podsiadlowski et al. 1995). As these reactions take place at base of the convective envelope, fusion products can be mixed to the surface. Here we review the main nucleosynthetic outputs.

Lithium Production: The hot temperatures and strong convection within TŻOs allows the synthesis of Li through the Cameron-Fowler mechanism (Cameron 1955). ${}^7\text{Be}$ is first created and then rapidly mixed into an area with cooler temperatures where it captures an electron to form ${}^7\text{Li}$. Because TŻO lifetime constraints are comparable to the depletion timescale for ${}^3\text{He}$ ($\sim 10^5$ years), large quantities of Li should build up and be present at all times (Podsiadlowski et al. 1995).

The irp-process and Heavy Element Synthesis: The temperature in the atmosphere of the NS in a TŻO is very high ($\sim 10^9$ K), which, when coupled with the convective atmosphere, leads to the interrupted rapid proton (irp) process. Large abundances of elements such as Zn, Br, Rb, Y, Zr, Mo, and Ru will be dredged to the surface (Cannon 1993). Biehle (1994) found that Mo should be enhanced relative to Solar by a factor >1000 and Rb by a factor of ~ 200 .

Calcium Production: Finally, Levesque et al. (2014) observed a higher Ca/Fe ratio in HV 2112 than a control sample of RSGs. While Ca is not directly synthesized within a TŻO, Ca from the core of the companion star could be mixed upwards during the formation of the TŻO (Tout et al. 2014).

Summary: Should any of the HLOs or HAVs be TŻOs, we would expect to see enhancements in both Li and heavy elements, with higher Mo abundances than Rb.

5.1.2. Massive and Super-AGB Spectra Predictions

There are multiple stages in the m/s-AGB phase, which formally begins after core-helium exhaustion: (i) in the *early AGB phase* stars undergo helium shell burning, (ii) eventually, the convective layer will penetrate the helium-rich zone and the *second dredge-up* (2DU)

will mix H-burning products to the surface and, finally (iii) there is a *thermally-pulsing (TP) stage* with a thermally-unstable He-burning shell. The TP-AGB stage can be accompanied by the *third dredge-up* (3DU) where He-burning products are mixed to the surface. In sAGB stars, carbon burning also ignites off-center *prior* to the TP phase. There are multiple points in this evolution leading to enhanced surface abundances of various elements. Here we review the main nucleosynthetic processes and their mass dependence.

Hot Bottom Burning and Li Production: In both massive and super-AGBs, a thin layer at the base of the convective envelope becomes so hot after the 2DU that H-burning reactions take place, a process known as Hot-Bottom Burning (HBB, Sackmann & Boothroyd 1992; García-Hernández et al. 2013). This triggers the Cameron-Fowler mechanism (Cameron 1955; Cameron & Fowler 1971), and large quantities of Li are carried to the surface. This Li is continually destroyed, and new production ceases when the supply of ${}^3\text{He}$ has been depleted. As a result, the period of Li enhancement is generally expected to be short-lived ($\sim 10^4 - 10^5$ years; Doherty et al. 2014b) with little to no Li remaining as the star nears the end of the TP-AGB. However, the duration of the Li rich phase increases and the time of peak Li enrichment occurs later for lower mass AGBs (García-Hernández et al. 2013; Karakas & Lugaro 2016). The minimum mass required to instigate HBB depends on a number of factors, including metallicity. García-Hernández et al. (2007) predict HBB occurring for $M > 3M_{\odot}$ at LMC metallicity, while Karakas et al. (2018) finds $M > 3.75M_{\odot}$ at SMC metallicity.

The s-process and Heavy Element Synthesis: Once the TP-phase begins, 3DU events bring heavy elements, synthesized in the intershell region by the slow (s) neutron capture process, to the surface. In massive ($M > 4M_{\odot}$) AGB stars, the primary source of free neutrons is the ${}^{22}\text{Ne}(\alpha, n){}^{25}\text{Mg}$ He-burning reaction (Abia et al. 2002; van Raai et al. 2012; Karakas et al. 2012). The high density, but short lifetime, of ${}^{22}\text{Ne}$ leads to an abundance pattern with higher production of $Z=36-40$ elements compared to heavier $Z > 40$ elements (see Doherty et al. 2017 Figure 10), with a strong peak at Rubidium ($Z=37$; García-Hernández et al. 2006). Generally, the Rb abundance is expected to peak for mAGB stars and then decrease slightly for the higher mass sAGB stars (Karakas et al. 2018; Ritter et al. 2018).

The i-process and Heavy Element Synthesis: In the *most* massive super-AGB stars (top $\approx 0.3M_{\odot}$), a process called *dredge-out* can occur where a flux of protons is mixed into the He-burning zone near the end of the C-burning phase (Ritossa et al. 1999). This subsequently

leads to a high enough density of free neutrons (Doherty et al. 2017 §2.3.2) to trigger the intermediate (i) neutron capture process. Although the exact i-process abundance pattern has yet to be calculated (Doherty et al. 2015; Jones et al. 2016), it is possible that the high neutron densities could lead to higher abundances of heavier elements ($Z > 40$), such as Mo ($Z = 42$), than the Ne^{22} driven s-process described above.

Simultaneous Li and s-process elements: Since the strong increase in Li after the 2DU is expected to be depleted over time, and s-process elements are only starting to build up in the thermally pulsing phase with the 3DUs, we might not expect sAGBs to show simultaneous enhancements in both. However, concurrent mild enhancement in Li and s-process elements has been observed in stars by Smith et al. (1995). Tout et al. (2014) explain that a period mild Li and s-process enhancement is possible for 10^4 - 10^5 years (van Raai et al. 2012; Doherty et al. 2014b) during the first few thermal pulses before the Li is completely destroyed. This would be more common for lower mass AGB stars, as the period of Li enrichment lasts longer (Karakas & Lugaro 2016). Mazzitelli et al. (1999) also explain this phenomena as due to the 3DU already having occurred by the first thermal pulse.

Calcium Production: Ca is not a typically expected product of nucleosynthesis in sAGBs (e.g. Tout et al. 2014). It is possible that HBB could lead to the synthesis of a small amount of Ca (Ventura et al. 2012), but this is poorly constrained.

Summary: In conclusion, AGB stars with masses above $M \gtrsim 4M_{\odot}$ should be enhanced in both Li and s-process elements, with an abundance peak at Rb. The former peaks in the *early* TP phase and the latter in the *late* TP phase, but a brief period ($\lesssim 10^5$ years) of moderate enhancement in both is possible, especially in lower mass AGBs. Elements heavier than Rb (i.e. Mo) will not be as strongly enhanced. Other than the potential for i-process enhancement in the *most* massive sAGB stars, there is no specific nucleosynthetic signature for the off-center carbon burning that formally defines a sAGB star (Doherty et al. 2017). Constraints on mass are therefore essential to distinguishing between mAGBs and sAGBs. The mass range of sAGBs is predicted to be ~ 6.5 - $12 M_{\odot}$ (Garcia-Berro & Iben 1994), though at low metallicities this lower bound can extend to $\sim 5M_{\odot}$ (Girardi et al. 2000; Doherty et al. 2017).

5.2. Method and Comparison Sample

In order to assess the possible enhancement of heavy elements and Li in the HLOs and HAVs we broadly follow the approach of Levesque et al. (2014) and Kuchner

Table 2.

Pseudo-Equivalent Width Ratio	Short Name
Li I 6707.91Å/Ca I 6572.78Å	Li/Ca
Li I 6707.91Å/K I 7698.97Å	Li/K
Mo I 5570.40Å/Fe I 5569.62Å	Mo/Fe
Rb I 7800.2Å/Ni I 7797.58Å	Rb/Ni
Rb I 7800.2Å/Fe I 7802.47Å	Rb/Fe
Ni I 7797.58Å/Fe I 7802.47Å	Ni/Fe
K I 7698.97Å/Ca I 6572.78Å	K/Ca
Ca I 6572.78Å/Fe I 5569.62Å	Ca/Fe

et al. (2002). The key elements we examine are Rb, Mo, and Li. We use the ratio of their pseudo-equivalent widths (p-EW) to a nearby line of Ca, K, Ni, or Fe. The ratios and rest wavelengths are shown in Table 2, where ‘control’ ratios are separated from ‘enhancement’ ratios by a horizontal line. We then compare these ratios, as a function of temperature to account for both the temperature dependent nature of spectral features and the intense line blanketing effects from TiO absorption bands, to a control sample of stars in order to determine if the HLOs and HAVs show evidence of enhancements. For our control sample we chose a population of RSGs from the sample of Neugent et al. (2012), following Levesque et al. (2014), since RSGs should not show enhancement in Li or s-/irp-process elements. These RSGs have temperatures and luminosities that span the range of possible HLO/HAV properties estimated in Paper I.

5.3. Observations and Data Reduction

5.3.1. Magellan MIKE Spectra

We obtained high-resolution spectroscopy of 27 stars (9 HLOs, 4 HAVs, and 14 RSGs) using the Magellan Inamori Kyocera Echelle (MIKE Bernstein et al. 2003) spectrograph on the 6.5-meter Magellan Clay telescope at Las Campanas Observatory, Chile. Observation dates and times are shown in Table 3, where HLOs, HAVs, and RSGs are separated by horizontal lines. Observations were made using 2x2 binning, ‘slow’ readout mode, and the 1” slit. HV 2112 was observed using the 0”7 slit. The spectral lines listed in Table 2 are all contained within the red arm of MIKE, which has a wavelength range of ~ 4900 - 9500\AA , pixel scale of $0”13/\text{pixel}$, and a resolution of $R = 22,000$ for the 1” slit.

We observed all HLOs from Paper I except for SMC-4 and LMC-5, which were near the dimmest point of their light curves during our observations and hence too faint to observe ($V > 16$ mag). The four HAVs observed

were among the subset that had their physical properties measured in Paper I. Finally, we observed 14 RSGs for the control sample described in §5.2, chosen to span a similar temperature range to the HLOs/HAVs (see § 5.6).

5.3.2. Data Reduction

Initial data reduction was performed using the CarPy MIKE pipeline³ (Kelson et al. 2000; Kelson 2003) which performs bias and flat field corrections, wavelength calibration, and extraction of individual echelle orders. The reduced data (including standard stars) is available online⁴ on Zenodo (European Organization For Nuclear Research & OpenAIRE 2013). We then normalize the spectra around each feature of interest using a low order polynomial with the IRAF (Tody 1986, 1993) task `continuum`.

5.3.3. Radial Velocity Determination

The heavy element lines we will analyze may be weak and are located in a forest of other metal lines in the spectra of these large, cool stars. To properly assess the presence of these elements, it is necessary to precisely correct our spectra to the rest frame. We carry out this process in three steps.

First we performed a heliocentric correction on each spectrum using the IRAF task `rvcorrect`. Second, we perform an initial correction for the radial velocity (RV) of the stars within the MCs, computed by cross correlating our spectra with a model template.

We measure this initial RV correction using the Ca II triplet (8498.02Å, 8542.09Å, 8662.14Å) and the IRAF package `fxcor`. For our template, we use a model spectrum from the PHOENIX library⁵ (Husser et al. 2013). Given the cool temperatures and large radii of our stars, we used a 3200 K, $\log(g)=0.0$ model, and corrected the model ‘vacuum’ spectrum to ‘air’ wavelengths.

All of the HLOs and HAVs display reverse P Cygni emission in the Ca II triplet (shown in Figure 4; discussed in § 5.4). This will naturally leave a small remaining shift when compared to templates with pure absorption, as the absorption component of a P Cygni feature is offset from the rest frame. Thus, after the initial RV correction was applied, we examined the Ca I 6572Å and Li I 6707Å lines, which are isolated and strong in almost all of the HLO/HAVs. We found these lines to be offset from their expected rest wavelengths by $\sim 5\text{--}20$ km/s. We therefore apply a second correction

to remove these offsets. For our RSG control sample (which do not show P Cygni features) we found that any offsets of the Ca I and Li I lines relative to the Ca II RV were very small ($\sim 0\text{--}4$ km s⁻¹). However, we applied the correction for consistency. In Table 3, we list the resulting RVs, which range from 93 – 188 km s⁻¹ in the SMC and 240 – 304 km s⁻¹ in the LMC. These values are consistent with being in the Magellanic Clouds (e.g. Neugent et al. 2010, 2012; Davies et al. 2018).

5.4. Basic Spectral Features

Here we present and describe the basic spectral features of the HLOs and HAVs as a population. In Figure 4 we highlight several regions of interest for all the HLOs and a subset of RSGs for comparison. Broadly, the spectra of the HLOs are consistent with expectations for cool, inflated stars. They display TiO blanketing (Fig 4; Panel D) along with a plethora of metal absorption lines. Those lines are narrow (mean Full Width at Half Maximum = $0.48 \pm 0.08 \text{Å}$, $\approx 22 \text{km/s}$), indicating both a low rotation rate and low surface gravity.

However, the spectra of the HLOs/HAVs are distinct from those of many other cool stars. They have Balmer emission with complex line profiles (Fig 4; Panel A), seen in all but HAV-1, and inverse P Cygni profiles in the Ca II triplet (Panel C), seen in all HLOs and HAVs. In contrast, the control sample of RSGs display pure absorption in both H and Ca II. Balmer emission was first noted in HV 2112 by Levesque et al. (2014).

Traditional P Cygni profiles, where the absorption is blue-shifted, are characteristic of outflows such as a stellar wind or expanding gas shell. An inverse P Cygni profile, with a red-shifted absorption component, *could* be indicative of in-falling material. Indeed, inverse P Cygni profiles are common features of Young Stellar Objects (Walker 1972; Calvet & Hartmann 1992; Hartmann et al. 1994) and have been detected in hot LBV stars (Wolf & Stahl 1990; Walborn et al. 2017). Both Balmer emission and inverse P Cygni lines have also been observed in some Mira variables (cool, pulsating, giants) where they have been linked to shocks propagating through the stellar atmosphere (Kudashkina & Rudnitskij 1994; Barnbaum & Morris 1993; Richter & Wood 2001)

In particular, we consider the Mira S Car, an AGB star with a similar effective temperature but a lower luminosity and a shorter period than HLOs/HAVs, studied in detail by Gillet et al. (1985). S Car displays complex Balmer features (H- α , H- β), inverse P Cygni lines (Ca II triplet, Fe I, and Ti I), and also doubled metal lines (K I and Fe I), which are nearly identical to the features in the HLOs/HAVs (see Figures 2-6 in Gillet

³ <https://code.obs.carnegiescience.edu/mike>

⁴ <https://zenodo.org/record/7058608>

⁵ <https://phoenix.astro.physik.uni-goettingen.de/>

Table 3. Spectroscopic observations.

Name	RA (J2000°)	Dec (J2000°)	Observation Date/Time ^a	Phase ^b	RV ($\frac{\text{km}}{\text{s}}$) ^c
SMC					
HV 2112	17.515856	-72.614603	2018-03-13-23:46:01	0.10	120±6
SMC-1	11.703220	-72.763824	2020-01-18-00:27:18	0.00	184±4
SMC-2	13.036803	-71.606606	2019-12-01-00:19:47	0.97	125±3
SMC-3	13.909812	-73.194845	2019-01-01-02:55:29	0.21	188±5
SMC-5	15.903689	-73.560525	2019-12-01-00:33:04	0.15	176±7
SMC-6	17.612562	-72.596670	2019-01-01-03:09:02	0.85	127±3
HAV-1	10.339302	-72.837669	2020-01-18-00:47:34	0.19	93±4
LMC					
LMC-1	80.824095	-66.952095	2019-01-01-03:57:19	0.07	278±3
LMC-3 ^d	84.986223	-69.589014	2020-01-18-01:52:56	0.63	286±2
LMC-4	86.709478	-67.246312	2019-01-01-04:31:36	0.88	304±2
HAV-2	74.731359	-66.761542	2020-01-18-02:24:23	0.22	269±3
HAV-3	81.092362	-66.110381	2020-01-18-03:20:52	0.13	291±3
HAV-4 ^d	85.173783	-66.246323	2020-01-18-05:35:12	0.09	278±13
RSG-1	73.840208	-69.787972	2019-01-01-05:47:41	N/A	256±5
RSG-2	73.883208	-66.843861	2019-01-01-06:02:08	"	299±6
RSG-3	74.202083	-69.665250	2019-01-01-05:37:25	"	251±9
RSG-4	76.174125	-70.710333	2020-01-18-03:09:25	"	246±6
RSG-5	81.501417	-71.596889	2020-01-18-04:40:39	"	240±5
RSG-6	81.947792	-69.222361	2019-01-01-06-12-10	"	274±5
RSG-7	82.189500	-69.967305	2019-01-01-06:23:19	"	274±7
RSG-8	82.418041	-66.838028	2020-01-18-04:48:07	"	302±4
RSG-9	82.814917	-69.066333	2020-01-18-04:55:35	"	270±6
RSG-10	83.209667	-67.462583	2020-01-18-05:02:27	"	290±4
RSG-11	83.886833	-69.071833	2020-01-18-05:10:42	"	292±5
RSG-12	84.942708	-69.324471	2020-01-18-05:18:13	"	246±6
RSG-13	85.102000	-69.354610	2020-01-18-05:26:28	"	262±7
RSG-14	85.271083	-69.078417	2019-01-01-06:33:19	"	253±6

^aUTC Time at beginning of observation

^bApproximate phase of the variability curve the HLO or HAV was at when the observation was taken, with 0.0 = peak of light curve and 0.5 = trough.

^cRadial Velocity correction. See §5.3.3 for details.

^dLMC-3 and HAV-4 are at lower luminosities than the other members of their respective classes, but are included for comparative purposes.

et al. 1985). In Figure 5 we display these features for HV2112. Gillet et al. (1985) argue that these features are the result of ballistic motions stemming from a passing shock. In their picture, the features are not due to in-falling material, but strong absorption lines with a central emission line. If the emission is weak, the feature appears as a double line, while if it is strong, it produces an inverse P Cygni profile.

We therefore posit that the features described in this section are analogous to those in Gillet et al. (1985) and are not indicative of in-falling matter, but of complex motions in the photosphere of the stars due to pulsation-driven shock waves. This is consistent with the high amplitudes of the light curves for these objects. In particular, these complex emission features are expected near photometric maximum phase, which matches the timing of our spectra, though spectra taken near the photomet-

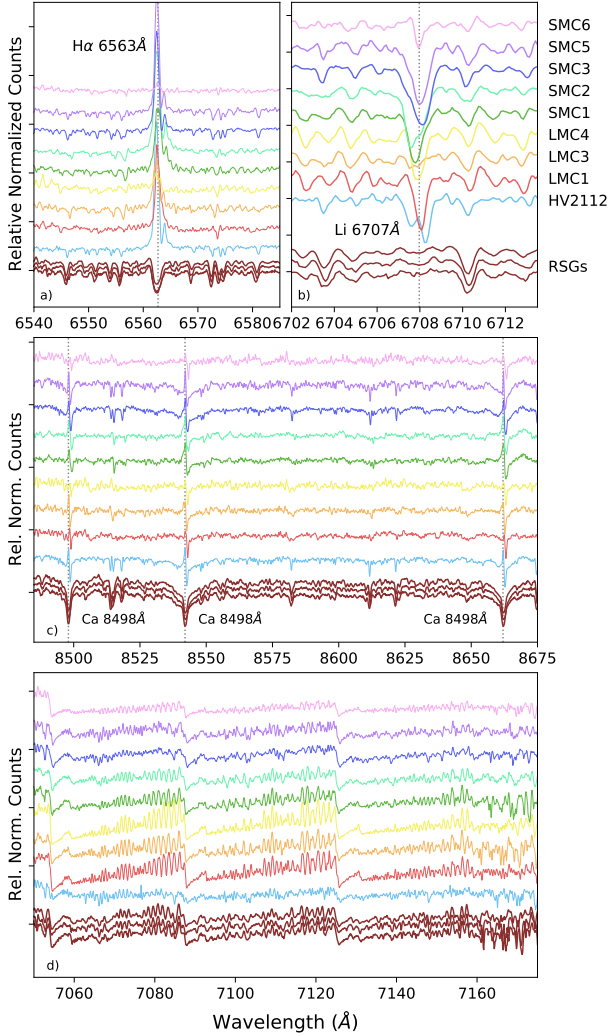


Figure 4. Spectra of all the observed HLOs and 3 RSGs (RSG-2, -8, and -13) showing various spectral features. Panel a) shows the H- α 6563Å feature, panel b) shows the Li 6707Å feature, panel c) shows the infrared calcium triplet, and panel d) shows an area of TiO blanketing. The HLOs are labelled on the right side of panel b).

ric minimum would be required to confirm this. The light curves of the HLOs also have bumps in the ascending phase (Paper I Figure 4), which have also been linked to shocks (Kudashkina & Rudnitskij 1994). While the HAVs do not explicitly show this double-peaked feature in their light curves (Paper I Figures 17-18), they may just be too weak or faint to see in the ASAS-SN (All-Sky Automated Survey for SuperNova) data. The lack of a double peaked light curve also does not specifically exclude the presence of shocks.

5.5. Pseudo-Equivalent Width Measurements

To assess the presence of heavy elements in the spectra of the HLOs/HAVs we measured the p-EWs for the fea-

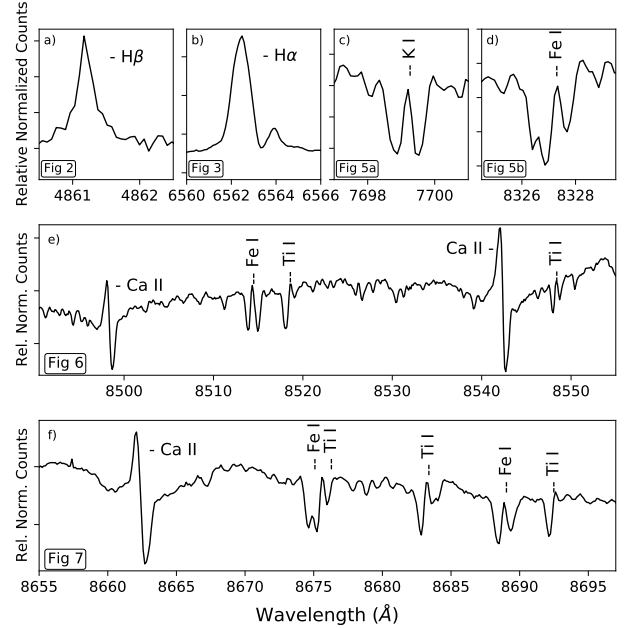


Figure 5. Spectral features of HV2112: The H β line (a), the H α line (b), the K I doubled lines (c), the Fe I doubled lines (d), and the Ca II triplet (e and f). The annotations in the bottom left of each panel indicate the Figure number in Gillet et al. (1985) for comparison.

tures listed in Table 2. Here we describe our procedure and details for specific lines.

We fit a Gaussian (or multiple Gaussians in the case of blended lines) to each line of interest. The local continuum level was determined by taking the mean of the data surrounding the line after sigma clipping our normalized data. Initial guesses for the location, depth, and width of the Gaussian(s) were estimated, and then allowed to vary within constraints ($\pm 0.1\text{\AA}$ for location, ± 0.1 normalized flux for depth, and a maximum width of 0.25\AA). Line locations were taken from the Atomic Line List (AtLL, van Hoof 2018) and the NIST Atomic Spectral Database (NIST ASD, Kramida et al. 2021).

To determine the errors on our measurements, we use a Monte Carlo approach. We generate 100 versions of each spectral segment by allowing each point to vary within its measurement uncertainty, and repeat the continuum determination and Gaussian fitting procedure. From this, we have 100 measurements of the equivalent width for each of the lines of interest. We report the mean of this distribution as our p-EW value, and its standard deviation as the uncertainty. These values are given in Table E3 in Appendix E. Details on specific line measurements are outlined in Appendix F.

5.6. Temperature Measurements

We want to compute the equivalent width ratios as a function of stellar temperature. For our control sample of RSGs, we simply use temperatures from the source catalog (Neugent et al. 2012).

For the HLOs and HAVs, we must account for the fact that their temperatures vary by ~ 300 K throughout their pulsation periods (Paper I). We first estimate the light curve phase at the epoch when the spectra were obtained by extrapolating the period of variability and peak of the ASAS-SN light curves presented in Paper I. These extrapolated phases are listed in Table 3, where a phase of 0.0 is the peak of the folded light curve, which corresponds to the hottest temperature, and a phase of 0.5 is the dimmest point, which corresponds to the coolest temperature. Excluding LMC-3, all spectroscopic observations were taken within the first quarter (0.0-0.25) or last quarter (0.75-0.99) of the variability cycle. We estimate the effective temperature at the time of the spectroscopic observation by linearly interpolating between the light curve phases based on the temperatures from Paper I. For each star we adopt a generic systematic uncertainty for these temperatures by taking the average of all temperatures in either the first or last quarter of variability, corresponding to the approximate phase at the time of observation (Table 3). These values are given in Table E3 in Appendix E.

5.7. Element Ratio Results

In Figures 6 and 7 we show the ratios of the p-EWs as a function of effective temperature for the HLOs, HAVs, and RSGs. Figure 6 shows ratios containing Li, Mo, and Rb, which should be enhanced in both TZO and sAGB stars relative to RSGs, though Mo is expected to be less enhanced than Rb for sAGBs, and Figure 7 shows the control ratios that do not contain these elements. In all panels, contours show the 1-, 2-, and 3- σ regions of the distribution of the RSG control sample. The density distribution was estimated by applying a kernel density estimator to the RSG sample. We first summarize these results for the HLOs and HAVs as a population and then compare our results for HV 2112 to those of Levesque et al. (2014) and Beasor et al. (2018).

5.7.1. Broad Trends Among the HLO/HAV Population

We consider a star to have a “clearly strong line” in absorption for a given element – relative to the control sample – if the equivalent width ratio falls above the 3- σ contour of the RSG control sample. For both lithium and rubidium we consider two different line ratios (Table 2). We refer to the potential enhancement of these elements as “ambiguous” if it falls above the 3- σ threshold in one of these ratios but not the other. Evaluating these plots generally, the HLOs and HAVs fall into four

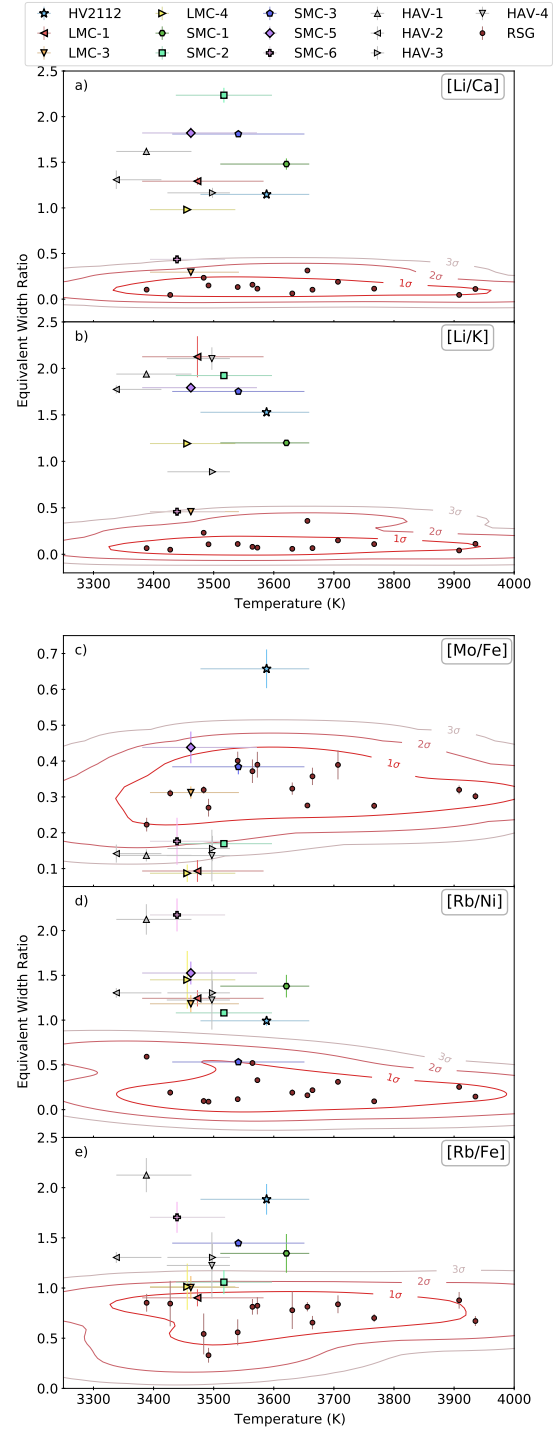


Figure 6. Pseudo-equivalent width ratios as a function of effective temperature for Li/Ca (a), Li/K (b), Mo/Fe (c), Rb/Ni (d), and Rb/Fe (e). The HLOs are shown with a variety of colors and markers as indicated in the legend. HAVs are shown in grey with different markers. RSGs are shown as dark red circles. The red lines are the 1-, 2-, and 3- σ contours for the distribution of RSGs modeled with a kernel density estimator. Any star not appearing in a panel is explained in the text.

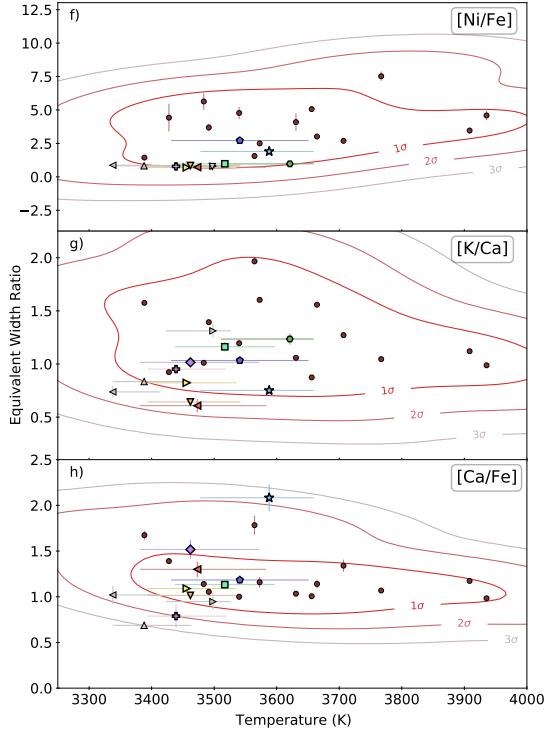


Figure 7. The same as Figure 6, but for the control ratios of Ni/Fe (f), K/Ca (g), and Ca/Fe (h).

broad categories, which we will relate to theoretical expectations in §5.8:

- Stars with clearly strong lines in Li, Rb, and Mo – HV 2112 only
- Stars with clearly strong lines in Li and Rb that lack a clearly strong Mo line – SMC-1, SMC-5, all 4 HAVs
- Stars with a clearly strong Li line and ambiguous Rb line that lack a clearly strong Mo line – SMC-2, SMC-3, LMC-1, LMC-4
- Stars with either a clearly strong or ambiguous Rb line that lack a clearly strong line in either Li or Mo – SMC-6, LMC-3.

The majority of the HLOs and HAVs clearly show increases in Li/Ca and Li/K compared to the RSG control sample in Figure 6 (panels a and b). For ratios containing heavy elements, the results are more varied. The only star to show an excess in Mo/Fe relative to the RSG sample is HV 2112 (panel c). Most of the HLOs and HAVs also show an increase in Rb ratios compared to RSGs (panels d and e), but some do not exceed the 3σ level in both the Rb/Fe and Rb/Ni ratios. For the control elements show in Figure 7, all of the HLOs and HAVs show similar p-EW ratios to the RSGs. The only

exception is that HV 2112 shows a slight (between 2- and 3σ) Ca/Fe excess. These results are summarized in Table 4.

The control sample RSGs are all located in the LMC, while the HLOs/HAVs are located throughout both Clouds. To investigate any bias this could introduce, we visually compare the location of HV 2112 relative to the control sample of RSGs both in our Figures 6-7 and in Figure 1 of Levesque et al. (2014, who compare to SMC RSGs). No strong differences can be seen. We additionally do not see any systematic differences between the LMC and SMC HLO/HAV stars in our analysis.

There are three cases where a star has not been included in a panel of Figures 6-7 because difficulties in fitting the local continuum lead to very low signal-to-noise ratios for the p-EW. SMC-1 is not included in the Mo/Fe (6c) and Ca/Fe (7h) panels due to a low signal-to-noise ratio for Fe I 5569Å. SMC-5 is not included in the Rb/Fe (6e) and Ni/Fe (7f) panels due to a very low signal-to-noise ratio for Fe I 7802.47Å. HAV-4 is not included in the Li/Ca (6a), K/Ca (7g), and Ca/Fe (7h) panels due to a low signal-to-noise ratio for Ca I 6572.78Å.

5.7.2. Comparison to Levesque et al. (2014) Measurements of HV 2112

Levesque et al. (2014) performed a similar spectroscopic analysis on HV 2112. Some quantitative differences are apparent in our measured p-EW ratios, likely due to a combination of physical (e.g. our spectra were obtained at a slightly different light curve phase) and systematic (e.g. we use different techniques for estimating the local continuum; treatment of doublets) effects. However, our overall results are broadly consistent: we both observe significant excesses in Li/Ca and Li/K relative to the RSG control sample and more moderate (but $>3\sigma$) increases in Mo/Fe and Rb/Ni.

We highlight two areas where our results differ slightly. First, we detect a clear high ratios in *both* Rb/Ni and Rb/Fe in HV 2112, while Levesque et al. (2014) observe only the former—which was noted as unusual. This seems to be driven by the large Rb/Fe ratio for the RSG control sample in Levesque et al. (2014, $\sim 2\text{-}4 \text{ \AA}$) compared to this work ($\sim 0.25\text{-}0.75 \text{ \AA}$). This difference may be due to the presence of an Fe I line close to Rb I $\lambda 7800.23 \text{ \AA}$ as discussed in Appendix F. In our analysis we fit a double Gaussian to this blended feature and attribute only the redder component to Rb. Second, while HV 2112 shows the highest Ca/Fe ratio of any star in our sample, this translates to only a slight excess ($2\text{-}3\sigma$) compared to the RSG control sample. In contrast, Levesque et al. (2014) find a clear ($>3\sigma$) enhancement relative to their RSG sample.

Levesque et al. (2014) also reported no enhancement in the Ba II 4554 Å line, another product of the s-process (Vanture et al. 1999). We visually inspected this line and similarly found that it was not enhanced in any of our stars relative to the RSG sample. However as mentioned in §5.1.2, elements with $Z > 40$ are not expected to be as enhanced as lighter $Z=36-40$ elements. For the considered metallicity range, the Ba ($Z=56$) production due to the Ne^{22} neutron source in m/sAGB stars is predicted to be very small, with values typically less than that of Mo ($Z=42$, see again Figure 10 of Doherty et al. 2017).

5.7.3. Comparison to Beasor et al. (2018) Measurements of HV 2112

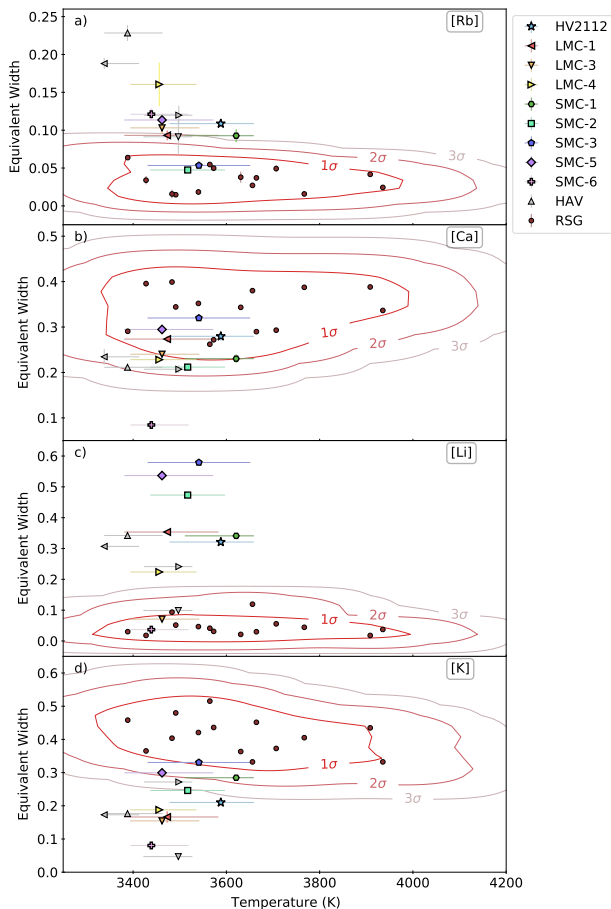


Figure 8. Plots of pseudo-equivalent width versus temperature for Rb, Ca, Li, and K. The colors, shapes, and contours are the same as Figures 6-7. This plot can be compared with Figure 2 of Beasor et al. (2018)

Beasor et al. (2018) also assess the spectrum of HV 2112 and conclude that there is *lack* of evidence for unusual abundances in either Rb or Ca, while a strong absorption in Li is observed and Mo is not discussed. Examining these results, we find that our overall con-

clusions are actually broadly consistent. Our different “headline” statements can be traced primarily to our choice of comparison sample—and hence what we are assessing an “enhancement” relative to.

Beasor et al. (2018) select comparison stars to have as similar luminosities and spectral types to HV 2112 as possible, as opposed to RSGs specifically. As a result, their comparison sample includes several relatively luminous AGB stars—which may themselves be enhanced in Rb and/or Li depending on their evolutionary state (see § 5.1.2). In particular, we note that of the three comparison stars that show Rb p-EWs larger than HV 2112 in Beasor et al. (2018), two were identified as HAVs in Paper I (HV 1719, HV 12149) and the third (HV 11417) would have been a candidate except that the amplitude of its V-band variability fell just below our cutoff of 2.5 mag. They are therefore members of the overall broad class of stars whose nature we are investigating. Four members of the Beasor et al. (2018) comparison sample have NIR colors consistent with RSGs, based on Boyer et al. (2011). HV 2112 does show a perceptibly higher Rb p-EW compared to those stars, although the difference is less significant than observed for Li.

As Beasor et al. (2018) consider p-EW values directly, rather than ratios, we plot the Rb, Ca, Li, and K p-EWs of our entire sample (HLOs, HAVs, and RSGs) as a function of temperature in Figure 8. Here we also see that HV 2112 shows strong absorption in both Li and Rb lines compared to the RSG control sample, though less extreme for Rb. In both cases HV 2112 is *not* the most extreme star: other HLOs/HAVs in our sample show larger p-EWs for both elements. In our data, we find that the HV 2112 Rb p-EW places it just above the 3σ contours for the RSG control sample, while in Beasor et al. (2018) it may be slightly less significant.

Similar to Beasor et al. (2018), we also find that if we consider the p-EW directly, HV 2112 does not show evidence for an excess in Ca. The $2\text{-}\sigma$ enhancement discussed above is evident only when considered in comparison to the nearby Fe line.

5.8. Interpretation of Element Ratio Results

Here we interpret the results of the p-EW ratio analysis in the context of expectations for TŻO and sAGB stars (see §5.1) for the four broad categories introduced in §5.7.1. To accompany the text, Table 4 lists all the p-EW ratios and whether each HLO/HAV shows a clear increase in that ratio when compared to the RSG control population. As the abundance predictions for both TŻO and sAGB stars in §5.1 are dependent on stellar mass, we also provide the HLO mass estimates from Paper I.

Table 4. Mass ranges & pseudo-Equivalent Width enhancements relative to RSGs.

Name	Mass Range (M_{\odot})	Li/Ca	Li/K	Mo/Fe	Rb/Ni	Rb/Fe	Ni/Fe	K/Ca	Ca/Fe
HV 2112	7.5–14.0	✓	✓	✓	✓	✓	X	X	~
SMC-1	4.5–6.0	✓	✓	N/A	✓	✓	X	X	N/A
SMC-2	4.0–10.5	✓	✓	X	✓	X	X	X	X
SMC-3	5.0–12.5	✓	✓	X	X	✓	X	X	X
SMC-5	2.5–6.0	✓	✓	X	✓	N/A	N/A	X	X
SMC-6	6.0–11.0	~	~	X	✓	✓	X	X	X
LMC-1	5.0–11.5	✓	✓	X	✓	X	X	X	X
LMC-3	2.0–4.0	X	~	X	✓	X	X	X	X
LMC-4	5.0–12.0	✓	✓	X	✓	X	X	X	X
HAV-1	N/A	✓	✓	X	✓	✓	X	X	X
HAV-2	N/A	✓	✓	X	✓	✓	X	X	X
HAV-3	N/A	✓	✓	X	✓	✓	X	X	X
HAV-4	N/A	N/A	✓	X	✓	✓	X	N/A	N/A

NOTE—See Figures 6-7 for more detail. ✓ denotes p-EW ratios higher than the 3- σ region of the RSG control sample, ~ denotes ratios between 2- and 3- σ , and X marks ratios below 2- σ . N/A denotes ratios not included due to a low signal-to-noise ratio (see text for details), and masses that were estimated in Paper I.

Strong Li, Rb, and Mo lines: HV 2112 shows larger p-EW ratios for all 3 elements compared to the RSGs, and it is the only star to show an enhancement in Mo/Fe. This could indicate a TŻO identity—increased surface abundances are expected for all of these elements in TŻOs. With an estimated mass of 7.5-14 M_{\odot} , HV 2112 also lies the closest to the theoretical minimum mass for TŻOs (~ 13 -15 M_{\odot}) of any of the HLOs/HAVs. However, Mo is expected to be enhanced by a factor of >5 more than Rb in TŻOs, which is not clear from our data. Alternatively, the mass constraints for HV 2112 are also consistent with the most massive sAGB stars. In this case, the simultaneous Li and s-process enhancements would require HV 2112 to be relatively early in the TP phase, before Li is significantly destroyed. Detailed abundance calculations would be required to determine if the Mo excess is consistent with an s-process abundance pattern (e.g. Doherty et al. 2017), or if HV 2112 is one of the *most* massive sAGB stars that might undergo i-process nucleosynthesis (Jones et al. 2016). Finally, the evidence for a Ca enhancement is modest. Ca is not traditionally expected as a primary burning product in either TŻOs or sAGBs, although there are explanations for an enhancement for both classes of stars (Tout et al. 2014; Ventura et al. 2012).

Strong Li and Rb lines: SMC-1, SMC-5, and all 4 HAVs show clearly large Li and Rb p-EW ratios compared to RSGs, with no similar increase in Mo/Fe. This is consistent with expectations for m/sAGB stars in the

TP phase. The estimated mass ranges of SMC-1 and -5 indicate that they are most likely massive rather than super AGB stars ($M_{max} \leq 6.0M_{\odot}$). The lack of an *observable* Mo enhancement is not unexpected, as its production is predicted to be practically negligible over this mass range, and at least a factor of ~ 3 lower than that of Rb (Doherty et al. 2017; Ritter et al. 2018; Karakas et al. 2018). The Rb excess coupled with a lack of observed Mo is difficult to reconcile with a TŻO origin as Mo should be significantly enhanced in a TŻO.

Strong Li and ambiguous Rb lines: SMC-2, SMC-3, LMC-1, and LMC-4 show strong absorption in Li, but only shows a $>3\sigma$ enhancement in one of the two Rb ratios. If these stars are enhanced in Rb they fall into the above category, and are likely sAGBs given their masses. If they are only Li-rich, then they may be m/sAGBs in the evolutionary phase after the 2DU when Li enhancement is at its peak, but before enough 3DUs/thermal pulses have taken place to dredge up a significant quantity of s-process material. García-Hernández et al. (2013) has examples of mAGBs with significant Li and little to no s-process abundance.

Strong Rb line and no Li ratio enhancement: SMC-6 does not show a *clear* excess in Li relative to the control sample. This is difficult to reconcile with a TŻO identity, as TŻOs are predicted to have strong Li enhancements throughout their entire lifetimes (Podsiadlowski et al. 1995). SMC-6 is the only HLO with a minimum estimate mass *above* the threshold where HBB should

occur in AGB stars ($M > 3-4M_{\odot}$) that does not show a significant excess in Li (although it *does* display a clear excess in Rb). This elemental signature would be consistent with a more evolved TP-AGB star (e.g. [Tabernero et al. 2021](#)). However, SMC-6 does *not* show signatures of strong mass loss, which should also set in later in the TP phase (Paper I). It thus is possible that SMC-6 is simply at a very narrow stage in evolution where Li has been mostly destroyed, but a delayed superwind has not yet occurred ([Vassiliadis & Wood 1993](#); [Doherty et al. 2014a](#)). In particular, it falls very close to the $3\text{-}\sigma$ line for the RSG control sample in both Li/Ca and Li/K in Figure 6.

Ambiguous Rb line and no Li ratio enhancement: LMC-3 has the lowest luminosity of any of the HLOs. Its lack of Li ratio enhancement is not necessarily surprising as its estimated mass $\sim 2-4M_{\odot}$ falls below the range where HBB is expected to occur. However, this mass also falls below the threshold where ^{22}Ne acts as the primary seed for the s-process, which is what leads to a heavy element abundance peaked at Rb. Thus, if LMC-3 is enriched in Rb (its line ratios were ambiguous) its mass may be underestimated and it would fall in the same narrow evolutionary phase as SMC-6.

In conclusion, to account for the possible s-process enrichment present in most of the sample, these stars must have undergone 3DU events. Most have not yet destroyed their Li enhancements. Finally, from Paper I, these stars lack strong mass loss rates ($\dot{M} \approx 10^{-7}M_{\odot}\text{yr}^{-1}$) and have not yet reached the superwind ($\dot{M} \geq 10^{-4}M_{\odot}\text{yr}^{-1}$) phase. Therefore, while multiple possibilities still exist for some individual stars, their spectroscopic properties paint a picture of the HLOs and HAVs being consistent with expectations for m/sAGB stars in the TP phase, but before the onset of the superwind.

6. IMPLICATIONS FOR THE NATURE OF THE SOURCES

The goal of this work was to use 4 methods to analyze the properties of HV 2112 and the population of similar stars identified in Paper I. Here we combine the results from all four parts of the paper: the analysis of the kinematic environment (§2), the local star formation histories (§3), the radio environment (§4), and the spectroscopic analysis of line ratios (§5), in order to discuss the collective evidence for classifying them as TŻOs or m/sAGB stars. We discuss HV 2112 individually in §6.4.

6.1. HLOs and HAVs as a class

Across the photometric analyses and estimation of physical properties in Paper I, the HLOs and HAVs displayed consistently similar features. This continues in

the kinematic, star formation history, radio, and spectroscopic analyses. This is consistent with our hypothesis that HLOs and HAVs are one class of stars, despite the difference in light curve shape.

6.2. Thorne-Żytkow Object Hypothesis

Taken together, the results of the four analyses are difficult to reconcile with a TŻO origin for the HLO/HAVs as a population. On the one hand, we do not see any evidence for either a large peculiar velocity or a supernova remnant at the location of any of the HLOs/HAVs. These results do not explicitly rule out a previous SN in the evolution of the stellar system as (i) TŻO progenitor systems have predicted recoil velocities ranging from $\sim 10\text{-}80\text{ km s}^{-1}$, similar to or below the general dispersion observed in the Magellanic Clouds and (ii) the radio lifetime of a typical SNR ($\sim 6 \times 10^4\text{ yrs}$) ([Frail et al. 1994](#)) is shorter than the estimated TŻO phase lifetime of $\sim 10^{5-6}\text{ yrs}$ ([Cannon 1993](#); [Biehle 1994](#)), though given the size of our population, it would be unlikely for us to observe zero SNRs. However, they also do not provide any specific evidence for a TŻO origin.

On the other hand, both the local star formation history and spectroscopic analysis pose a significant challenge for the TŻO hypothesis. Excepting HV 2112 (§6.4), as a population the HLOs/HAVs are associated with older stellar populations than $\sim 15\text{-}25M_{\odot}$ RSGs or short-period HMXBs. While this does not rule out a TŻO origin for any individual object, it is difficult to reconcile with the bulk population of HLOs/HAVs being the short lived descendants of these massive stars. Similarly, while most HLOs/HAVs appear to be Li-rich, as expected for TŻOs, the fact that many show an observable Rb excess but all stars except HV 2112 *lack* an observable Mo excess is counter to expectations from the abundance pattern predicted for the irp-process in TŻOs. In particular, Mo should be enhanced by a factor of >1000 compared to Solar abundances and Rb by a factor of ~ 200 ([Biehle 1994](#)).

We therefore conclude that the HLO/HAV population are not TŻOs. This is consistent with our interpretation from Paper I where we estimated their current masses to be below the $\sim 13\text{-}15M_{\odot}$ minimum for TŻOs.

6.3. Massive/super-AGB star Hypothesis

Taken together, our results are consistent with the HLOs/HAVs being a population of massive and super-AGB stars. First, the lack of a detectable peculiar velocity or SNR is consistent with an AGB interpretation. Second, while quantitative age-dating is complicated by the low number of objects in our sample and lack of quantifiable uncertainties, the star formation his-

tory analysis demonstrates that the HLOs/HAVs are associated with stellar populations that are most similar in age to luminous AGB stars.

Finally, as discussed in § 5.8 the spectroscopic features observed in the HLOs/HAVs can all be understood if they are massive ($M > 4M_{\odot}$) AGB stars at various points during TP phase, prior to the activation of a superwind. We emphasize that (i) the moderate enhancement in both Li and Rb can be achieved in the early-to-mid TP phase, especially for lower mass AGB stars, (ii) the presence of a *detectable* excess of Rb but not Mo is consistent with s-process nucleosynthesis in massive AGB stars, as the $^{22}\text{Ne}(\alpha, n)^{25}\text{Mg}$ reaction is the primary source of free neutrons and leads to an abundance pattern that peaks at Rb.

Based on the mass estimates from Paper I, the sample of HLOs and HAVs may contain both sAGB stars with $M \gtrsim 6-7M_{\odot}$, as well as mAGB stars (e.g. SMC-1, SMC-5, and LMC-3). The HLOs and HAVs appear to be a range of evolved, intermediate mass stars, ranging from the lowest masses that achieve HBB up through the highest mass of sAGB stars in HV 2112.

The identification of this population of m/sAGB stars has important implications to our understanding of stars near the supernovae mass boundary. In particular, based on their number statistics, this m/sAGB sample can increase our knowledge about the duration of the pre-superwind phase and hence early TP-AGB mass-loss rates, which in turn impacts the nucleosynthesis and stellar yields. Additionally, comparison to the observed maximum luminosities of the most massive AGB stars from this work may help constrain the very uncertain mixing length theory parameter α used within stellar evolutionary models during this phase.

6.4. HV 2112

HV 2112 remains the most exceptional star in our sample. It has the highest luminosity, variability amplitude, and inferred mass of all the HLOs (Paper I). It is the only star to show an extended structure in its radio environment. HV 2112 is the *only* HLO/HAV to show strong absorption in Mo as well as Li and Rb.

Many of HV 2112's properties are consistent with *both* a TŻO and sAGB classification. HV 2112 shows strong lines of Li and the s-process elements compared to RSGs, expected in both types of stars. The star formation rate of its local environment peaked $\sim 10^7$ years ago, though we cannot rule out that it was formed during an earlier, weaker burst of star formation. Finally, while we do not detect evidence of a previous supernova from the kinematic or radio environment of HV 2112, this does not rule out a TŻO nature.

There are three possible points of divergence: the estimated mass of HV 2112, its possibly enhanced calcium abundance, and the nature of the HI structure surrounding HV 2112. The estimated mass of HV 2112 from paper I ($7.5-14M_{\odot}$) is slightly below the minimum stable TŻO mass from Cannon (1993). On the other hand, sAGB stars should not have a Ca enrichment, and HV 2112 shows a small increase in Ca relative to K when compared to RSGs. Finally, while the structure surround HV 2112 (§4.4) is likely a random, unrelated ISM fluctuation (and thus not constraining to its origin) the possibility remains that it could be a small wind bubble blown by a $\sim 12M_{\odot}$ progenitor of a super-AGB star, which is consistent with the estimated mass range.

Assuming the HI structure is indeed a random ISM fluctuation, then if either the current mass of HV 2112 from Paper I is slightly underestimated *or* if the minimum stable mass for TŻOs (which is sensitive to the treatment of convection) is actually $< 15 M_{\odot}$ then HV 2112 would remain a strong TŻO candidate. In particular, Biehle (1994) speculates that the minimum mass of TŻOs should be $\sim 13 M_{\odot}$, just inside the estimated mass range of HV 2112. Additional modeling of TŻO structure and pulsation properties would enable better mass constraints and illuminate the nature of this star. Modern modeling of TŻOs may also revise other constraints; should updated theoretical predictions indicate longer TŻO lifetimes and a diversity of surface compositions, there would be no tension between our analyses and a TŻO identity for HV 2112.

However, if HV 2112 either does not have an overabundance of Ca (note the discussion in § 5.7.3) or if the speculation of Ventura et al. (2012) that small quantities of Ca could be produced in sAGB stars is true, then all the properties of HV 2112 are consistent with a super-AGB star near the beginning of the TP-phase. In particular the current mass estimate and observed excess in Mo would favor a sAGB at the upper end of the mass range and make it a candidate electron-capture supernova progenitor (Miyaji et al. 1980; Doherty et al. 2017).

7. SUMMARY & CONCLUSIONS

Motivation: Our goal in this paper was to clarify the nature of a population of super-AGB star candidates identified by O'Grady et al. (2020), and to see if any evidence supported a TŻO identity for any of the stars. We investigated their kinematics, local star formation history, and radio properties. Finally, we analyzed spectra of a subset of the sample to determine if the stars show evidence of Li and s- or irp-process enrichment.

Gaia Kinematics: We found no evidence of hyper-velocity stars in our sample, but were unable to conclusively rule out a lower ‘runaway’ or ‘walkaway’ velocity for any of the stars, mostly due to uncertainties on the proper motion measurements. Compared to the mean motion and dispersion of their local environment, our stars do not display significantly different proper motions. Uncertainties on proper motion measurements are expected to improve *significantly* by the end of the *Gaia* mission, therefore future releases will allow tighter constraints to be placed on the motions of these stars.

Local Star Formation History: We found that these stars are not associated with regions of recent star formation, and are more closely associated with stellar populations that will become AGB stars than those that will become RSGs.

Radio Environments: We saw no evidence of supernova remnants at the locations of the stars. A U-shaped structure exists around HV 2112, but it is most likely an unassociated, random fluctuation in the ISM.

Spectroscopy: HV 2112 displays significant Li, Rb, and Mo excesses, and a less significant Ca excess. All of the other stars in our sample have an Li excess, most have an Rb excess, and none show an excess in Mo or Ca compared to RSGs.

Population Final Conclusions: Collectively, the analyses do not provide any evidence pointing towards a TZO classification for these stars. Strong Li and Rb lines with weak Mo lines, relative to RSGs, and their estimated masses ($\sim 4-13M_{\odot}$) strongly indicates that these stars (except for HV 2112) are massive or super-AGB stars in the TP-AGB phase prior to the superwind onset. This would be the first population of super-AGB stars identified.

HV 2112 Final Conclusions: Due to an estimated mass too small to be a TZO, and a possible Ca enhancement which is not expected in sAGB stars, the true nature of HV 2112 remains ambiguous. If HV 2112 is not a TZO, given its cool temperature, very high luminosity, variability properties, and spectroscopic properties, it would most likely be a sAGB star. Better constraints on the mass and Ca abundance of HV 2112, as well as progress in theoretical modelling of TZOs are needed to fully determine its true nature.

ACKNOWLEDGMENTS

The authors thank: Emma Beasor, Jo Bovy, Ben Davies, Nancy Ramage Evens, Emily Levesque, Chris Matzner, Phil Massey, Nidia Morrel, Krzysztof Stanek, Todd Thompson, and Dennis Zaritsky for helpful discussions; Dan Kelson, Jennifer Laing, Adiv Paradise, and Ayushi Singh for technical help; Tana Joseph & Miroslav Filipovic for access to ASKAP-EMU images; Naomi McClure-Griffiths for access to SMC HI data. We thank the referee for helpful comments on the manuscript.

Spectroscopic data in this paper was obtained at the 6.5m Magellan Telescope at Las Campanas Observatory, Chile. The authors would like to thank all of the staff at LCO for their expertise and help.

The authors at the University of Toronto acknowledge that the land on which the University of Toronto operates is the traditional territory of the Huron-Wendat, the Seneca, and the Mississaugas of the Credit River. They are grateful to have the opportunity to work on this land.

The Dunlap Institute is funded through an endowment established by the David Dunlap family and the University of Toronto.

A.J.G.O. acknowledges support from the Lachlan Gilchrist Fellowship Fund. MRD acknowledges support from the NSERC through grant RGPIN-2019-06186, the Canada Research Chairs Program, the Canadian Institute for Advanced Research (CIFAR), and the Dunlap Institute at the University of Toronto. B.M.G. acknowledges the support of the Natural Sciences and Engineering Research Council of Canada (NSERC) through grant RGPIN-2022-03163, and of the Canada Research Chairs program. CSK is supported by NSF grants AST-1908570 and AST-1814440. B.J.S. is supported by NSF grants AST-1907570, AST-1908952, AST-1920392, and AST-1911074.

Support for this work was provided by NASA through the NASA Hubble Fellowship Program grant #HST-HF2-51457.001-A awarded by the Space Telescope Science Institute, which is operated by the Association of Universities for Research in Astronomy, Inc., for NASA, under contract NAS5-26555.

This research has made use of the following software:

Software: [astropy](#) ([Astropy Collaboration et al. 2018](#)), [IRAF](#) ([Tody 1986, 1993](#)), [TOPCAT](#) ([Taylor 2005](#)), [MARCS](#) ([Gustafsson et al. 2008](#))

APPENDIX

A. KINEMATIC DISTRIBUTION OF TOTAL PROPER MOTION RELATIVE TO THE LOCAL MEAN

We also assess the magnitude of the total proper motion of the HLOs/HAVs relative to their local environments. After subtracting the weighted means listed in Table 1, all of the HLOs except LMC-1 have residual proper motions of $0.1\text{--}0.3\text{ mas yr}^{-1}$. In Figure A1 we show where the HLOs lie relative to the cumulative distribution of all the nearby stars. Four HLOs (40%) fall within the inner 50% of the 1-D CDF, while 4 (40%) also fall in outer 25%. For the HAVs, 12 (44%) and 7 (26%) fall within the inner 50% and outer 25% of their local CDFs, respectively.

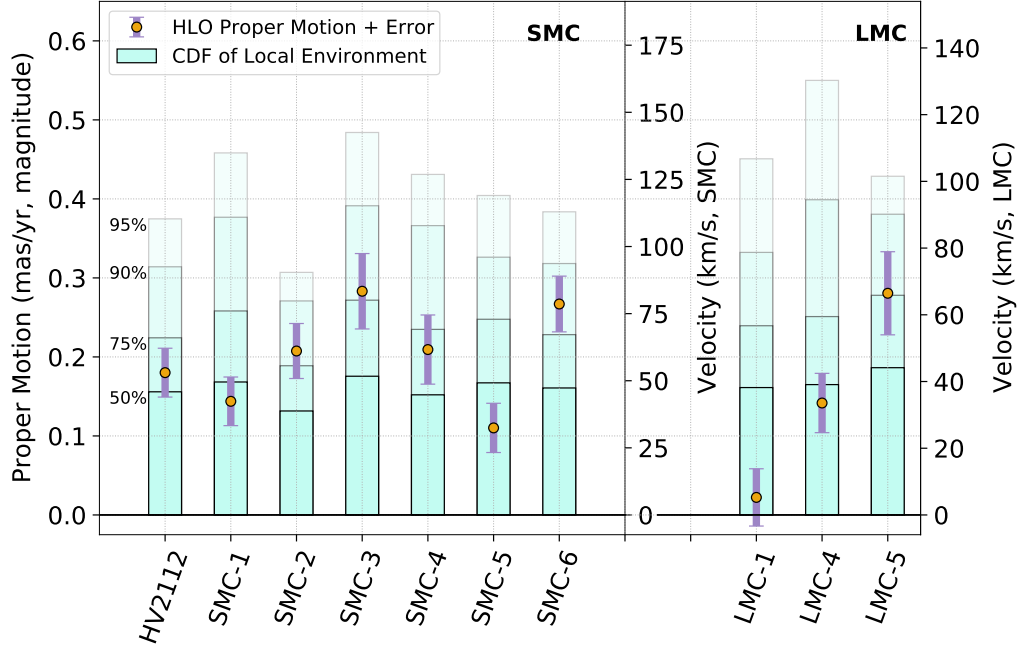


Figure A1. A comparison of the magnitude of the HLO proper motion to their local environments. The motion of the S/LMC and the weighted mean proper motion for the $5'$ area around each HLO has been subtracted, removing bulk motion and allowing the proper motion of each HLO to be compared to the average dispersion of their local environment. The segmented light blue bars denote 50/75/90/95% of the cumulative distribution function. The magnitude of the proper motion and associated measurement uncertainty are plotted for each HLO as a gold circle and violet error bar. Velocities (for SMC and LMC distances) are shown on the right axes.

In order to ascertain whether the fraction of HLOs/HAVs that fall in the outer regions of their local CDFs is actually higher than would be expected given the quality of their astrometric solutions, we performed the same analysis with a sample of other stars throughout the Magellanic Clouds. In each galaxy we randomly chose 10 test stars with two constraints: the star had to (i) be a probable Cloud member, and (ii) have astrometric excess noise in the range $0.2 < \epsilon_i < 0.5$ with a significance $D > 2$ (the same ϵ_i as the sample of HLOs). We then queried *Gaia* EDR3 for all stars within $5'$ of each test star, removed foreground contamination, and determined the location of the star within its local total proper motion CDF.

We ran this trial 500 times in each Cloud and found that in $\sim 54\%$ of these trials, 4/10 sources lie in the outer 25% of the 1-D CDF. This is similar to the results of the 10 HLOs. Thus, we do not see evidence that the HLOs have unusual total proper motions relative to their local mean.

B. SFH CEPHEID TEST

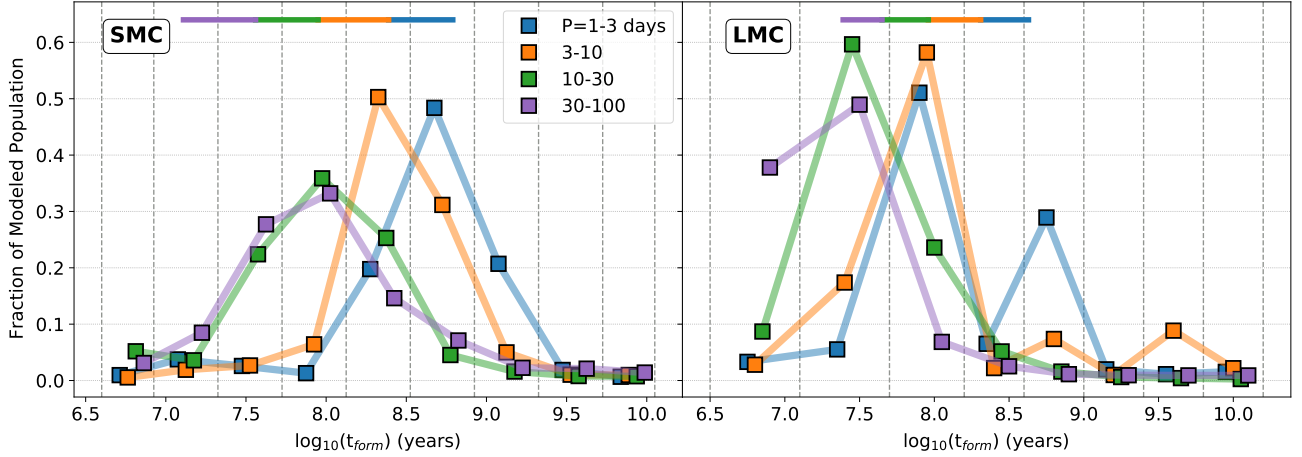


Figure B2. The same as Figure 2 but plotting a population of OGLE-III Cepheid variables. The populations are organized by variability period: 1-3 days in blue, 3-10 days in orange, 10-30 days in green, and 30-100 days in violet. The expected age range for each set of periods, calculated from Anderson et al. (2016), is shown as a colored bar at the top of the plot.

C. SFH QUANTITATIVE LIKELIHOODS

Here we quantify the similarity in star formation history of stellar populations by computing three likelihoods. We first find the maximum likelihood models for population 1 and 2, L_1 and L_2 . Then we find the maximum likelihood model $L_{12} = L'_1 L'_2$ for modeling them simultaneously assuming they have the same association with stellar ages by computing their likelihoods L'_1 and L'_2 for the same ϵ_i and maximizing L_{12} . We renormalize the ϵ_i for the two populations separately since they will generally contain different numbers of objects. The logarithmic difference, $\Delta \ln L = \ln L_{12} - \ln L_1 - \ln L_2$ is then a quantitative estimate of their similarity, yielding $\Delta \ln L = 0$ if there age distributions are identical. For test problems with 50 stars randomly distributed following the star formation rate at a fixed age, this approach robustly identifies random samples with the same age even though the random realizations of the populations are different. In Table C1 we present the likelihoods for all populations shown in Figure 2. The populations with the smallest $\Delta \ln L$ values for the HLOs and HAVs are AGB stars and not RSGs or associated high-mass phenomena (SNRs/HMXBs). This is consistent with our analysis in §3.

Table C1. Likelihood of similarity for observed populations

Sample	HLO			HLO+HAV		
	LMC	SMC	Tot	LMC	SMC	Tot
HLO	-0.202	0.001	-0.202	1.264	-0.011	1.253
HLO/HAV	1.382	-0.054	1.328	-0.182	-0.124	-0.306
O Rich AGB	2.672	0.403	3.075	2.607	0.372	2.978
low L O Rich AGB	2.633	0.020	2.654	2.854	0.173	3.027
high L O Rich AGB	2.731	0.150	2.881	4.336	1.224	5.560
RSG	5.976	1.959	7.934	20.162	3.890	24.052
SNR	2.942	3.554	6.496	5.396	6.071	11.467
HMXB	2.477	4.777	7.254	4.356	6.180	10.536

D. RADIO SURFACE BRIGHTNESS UPPER LIMITS

Table D2. Radio Surface Brightness Upper Limits

Name (HLO)	RA (deg)	Dec (deg)	ASKAP	ASKAP	ASKAP	ATCA	ATCA	ATCA
			887 MHz	960 MHz	1320 MHz	2734 MHz	4800 MHz	8600 MHz
SMC								
HV 2112	17.515856	-72.614603		0.2	0.4	0.6	0.8	4.5
SMC-1	11.703220	-72.763824		0.2	0.6	0.5	0.9	4.0
SMC-2	13.036803	-71.606606		0.2	0.3	0.5	0.8	4.7
SMC-3	13.909812	-73.194845		0.2	0.4	0.5	0.7	4.4
SMC-4	15.403412	-72.744751		0.2	0.5	0.8	0.9	3.9
SMC-5	15.903689	-73.560525		0.2	0.4	0.6	0.8	4.8
SMC-6	17.612562	-72.596670		0.3	0.4	0.5	0.8	4.6
	10.339302	-72.837669		0.2	0.4	0.5	0.8	4.6
	14.310338	-73.022591		0.6	1.2	0.9	0.9	4.8
	14.709024	-72.309883		0.5	0.6	3.3	0.9	3.7
LMC								
LMC-1	80.824095	-66.952095	0.6				0.8	4.4
LMC-3	84.986223	-69.589172	8.0				2.5	8.3
LMC-4	86.709478	-67.246312	0.4				1.3	4.3
LMC-5	88.116079	-69.236122	0.8				0.9	4.3
	68.98892	-70.997383	0.3				X	X
	70.108388	-71.661774	0.4				X	X
	73.436919	-68.966476	0.5				1.2	4.5
	74.370204	-70.458191	0.4				1.0	4.1
	74.731888	-66.76152	0.7				0.7	4.1
	75.349969	-70.098244	0.6				0.9	4.5
	76.517648	-70.28093	1.0				0.8	4.5
	76.615336	-68.201019	1.5				1.7	4.3
	76.664509	-71.599014	0.4				0.8	3.9
	76.909604	-69.735832	1.0				0.9	4.0
	77.999464	-71.606895	0.3				0.7	4.5
	78.92018	-66.08271	0.6				1.0	4.5
	79.793567	-70.972542	0.3				0.8	4.6
	80.006549	-67.578377	1.1				0.8	3.7
	80.79228	-67.835068	2.6				1.2	4.3
	81.092492	-66.110359	0.9				0.8	4.0
	81.138056	-70.71003	0.4				0.8	4.1
	82.323732	-67.042938	0.9				0.9	4.5
	83.249667	-70.68988	4.7				7.7	21.8
	85.173783	-66.246323	0.5				0.7	4.2
	87.305663	-70.711296	0.5				0.5	3.3
	87.980191	-71.078644	0.4				0.6	3.3
	89.684721	-68.447166	0.5				X	X
	91.290672	-72.676445	0.4				X	X

NOTE—Units: Σ_{1GHz} $1e-21$ W m^{-2} Hz^{-1} sr^{-1}

X denotes star outside of map boundaries

A blank space denotes the star not being in that map

E. TEMPERATURE AND PSEUDO-EQUIVALENT WIDTH VALUES

Table E3. Temperatures and pseudo-equivalent width values

Name	T_{eff} (K)	Fe 5569Å	Mo 5570Å	Ca 6572Å	Li 6707Å	K 7698Å	Ni 7797Å	Rb 7800Å	Fe 7802Å
HLOs									
HV 2112	3588^{70}_{110}	0.13±0.01	0.09±0.0	0.28±0.01	0.32±0.0	0.21±0.0	0.11±0.01	0.11±0.0	0.06±0.0
LMC-1	3473^{110}_{90}	0.21±0.01	0.02±0.01	0.27±0.01	0.35±0.01	0.17±0.02	0.07±0.0	0.09±0.01	0.1±0.01
LMC-3	3462^{80}_{70}	0.24±0.01	0.07±0.0	0.24±0.0	0.07±0.0	0.15±0.0	0.09±0.0	0.1±0.01	0.1±0.01
LMC-4	3456^{80}_{60}	0.21±0.01	0.02±0.01	0.23±0.0	0.22±0.0	0.19±0.0	0.11±0.01	0.16±0.03	0.16±0.02
SMC-1	3621^{40}_{110}	X	X	0.23±0.01	0.34±0.0	0.28±0.0	0.07±0.0	0.09±0.01	0.07±0.01
SMC-2	3517^{80}_{80}	0.19±0.01	0.03±0.0	0.21±0.01	0.47±0.0	0.25±0.0	0.04±0.0	0.05±0.0	0.04±0.0
SMC-3	3541^{110}_{110}	0.27±0.01	0.1±0.0	0.32±0.0	0.58±0.0	0.33±0.0	0.1±0.0	0.05±0.0	0.04±0.0
SMC-5	3462^{110}_{80}	0.19±0.01	0.09±0.01	0.29±0.01	0.54±0.01	0.3±0.0	0.07±0.01	0.11±0.01	X
SMC-6	3439^{80}_{50}	0.11±0.02	0.02±0.01	0.08±0.0	0.04±0.0	0.08±0.0	0.06±0.0	0.12±0.01	0.07±0.0
HAVs									
HAV-1	3388^{80}_{50}	0.31±0.01	0.04±0.0	0.21±0.01	0.34±0.0	0.18±0.0	0.11±0.01	0.23±0.01	0.13±0.01
HAV-2	3338^{80}_{0}	0.23±0.02	0.03±0.01	0.23±0.02	0.31±0.01	0.17±0.0	0.14±0.0	0.19±0.01	0.17±0.01
HAV-3	3498^{80}_{0}	0.22±0.02	0.03±0.01	0.21±0.01	0.24±0.01	0.27±0.0	0.09±0.0	0.12±0.01	0.11±0.01
HAV-4	3497^{30}_{80}	0.12±0.02	0.02±0.01	X	0.1±0.01	0.05±0.0	0.07±0.01	0.09±0.02	0.1±0.02
RSGs									
RSG-1	3388	0.174±0.005	0.039±0.003	0.291±0.003	0.03±0.003	0.458±0.001	0.108±0.001	0.064±0.002	0.075±0.007
RSG-2	3908	0.331±0.002	0.106±0.004	0.388±0.004	0.018±0.005	0.435±0.001	0.164±0.001	0.042±0.003	0.047±0.003
RSG-3	3767	0.363±0.002	0.1±0.003	0.387±0.004	0.044±0.003	0.405±0.003	0.17±0.002	0.016±0.001	0.023±0.001
RSG-4	3664	0.254±0.01	0.091±0.005	0.29±0.004	0.03±0.004	0.451±0.001	0.17±0.004	0.037±0.003	0.056±0.003
RSG-5	3572	0.235±0.012	0.091±0.007	0.272±0.003	0.031±0.006	0.436±0.002	0.151±0.004	0.05±0.004	0.061±0.004
RSG-6	3564	0.147±0.008	0.055±0.004	0.262±0.004	0.041±0.008	0.515±0.002	0.105±0.001	0.055±0.003	0.067±0.005
RSG-7	3655	0.378±0.004	0.104±0.002	0.38±0.002	0.119±0.001	0.332±0.001	0.169±0.0	0.027±0.001	0.033±0.001
RSG-8	3630	0.332±0.009	0.107±0.005	0.343±0.003	0.021±0.002	0.363±0.004	0.199±0.013	0.038±0.007	0.049±0.007
RSG-9	3706	0.219±0.011	0.085±0.008	0.293±0.003	0.056±0.008	0.373±0.005	0.158±0.007	0.049±0.005	0.059±0.003
RSG-10	3935	0.342±0.006	0.103±0.003	0.337±0.003	0.037±0.002	0.332±0.004	0.167±0.004	0.024±0.001	0.036±0.003
RSG-11	3491	0.327±0.011	0.088±0.008	0.344±0.003	0.052±0.005	0.48±0.002	0.165±0.004	0.015±0.003	0.045±0.003
RSG-12	3539	0.352±0.011	0.141±0.008	0.352±0.004	0.047±0.004	0.421±0.004	0.157±0.005	0.018±0.004	0.033±0.003
RSG-13	3427	0.285±0.004	0.088±0.003	0.396±0.007	0.018±0.004	0.365±0.002	0.178±0.017	0.034±0.005	0.04±0.009
RSG-14	3483	0.35±0.005	0.112±0.003	0.399±0.003	0.094±0.003	0.404±0.002	0.164±0.003	0.016±0.006	0.029±0.003

NOTE—RSG temperatures from (Neugent et al. 2012). Temperature and pseudo-equivalent width measurements described in §5.5.

F. NOTES ON SPECIFIC LINE MEASUREMENTS

K I: The K I 7698.97Å feature regularly appeared as a doublet in our observations. This doublet is thought to contain both stellar and interstellar components (Herbig & Soderblom 1982). The stellar component would have an RV similar to that LMC compared to the interstellar component. We take only the bluest component of the feature for all of our measurements.

Li I: Li I 6707.91Å often displays a blended Fe I 6707.43Å component (most obviously in HV 2112). We are careful to separate this Fe I line when possible and do not include it in the Li I measurement. Both NIST ASD and AtLL identify two lines of Li I in close proximity: 6707.76Å and 6707.91Å. We allow $\delta\lambda$ between the Li I 6707.91Å and Fe I 6707.43Å features to vary over 0.33–0.48Å.

Rb I: For Rb I 7800.23Å, AtLL reports a nearby line of Fe I at 7799.535Å. This partially blended line is clearly visible in the spectrum of HV 2112, and also appears throughout the rest of our data. We take care to separate this from the Rb I measurement. Finally, we found a shift in this Fe I–Rb I blend relative to the nearby Ni I 7797.58Å and Fe I 7802.47Å lines. When comparing our spectrum of HV 2112 to Figure 2 panel (e) of Levesque et al. (2014), the same pattern of lines is easily identifiable. However, throughout *all* of our spectra, the measured location of the

Fe I–Rb I blend is slightly redshifted when compared to the measured locations of the adjacent Fe I and Ni I lines (i.e. for Ni I 7797.58 and Rb I 7800.23, $\Delta\lambda > 2.65\text{\AA}$). For the HLOs and HAVs, Rb I is consistently $\sim 0.2\text{--}0.3\text{\AA}$ redder (a velocity change of $\sim 8\text{--}12$ km/s). For RSGs it is more pronounced, with a consistent shift of $\sim 0.55\text{--}0.65\text{\AA}$ redder ($\delta v \sim 21\text{--}25$ km/s). This may mean that the Fe I–Rb I absorption is from a different level of the photosphere than the adjacent Ni I and Fe I lines.

REFERENCES

- Abia, C., Domínguez, I., Gallino, R., et al. 2002, *ApJ*, 579, 817, doi: [10.1086/342924](https://doi.org/10.1086/342924)
- Anderson, R. I., Saio, H., Ekström, S., Georgy, C., & Meynet, G. 2016, *A&A*, 591, A8, doi: [10.1051/0004-6361/201528031](https://doi.org/10.1051/0004-6361/201528031)
- Antoniou, V., & Zezas, A. 2016, *MNRAS*, 459, 528, doi: [10.1093/mnras/stw167](https://doi.org/10.1093/mnras/stw167)
- Astropy Collaboration, Price-Whelan, A. M., Sipőcz, B. M., et al. 2018, *AJ*, 156, 123, doi: [10.3847/1538-3881/aabc4f](https://doi.org/10.3847/1538-3881/aabc4f)
- Auchettl, K., Lopez, L. A., Badenes, C., et al. 2019, *ApJ*, 871, 64, doi: [10.3847/1538-4357/aaf395](https://doi.org/10.3847/1538-4357/aaf395)
- Badenes, C., Harris, J., Zaritsky, D., & Prieto, J. L. 2009, *ApJ*, 700, 727, doi: [10.1088/0004-637X/700/1/727](https://doi.org/10.1088/0004-637X/700/1/727)
- Badenes, C., Maoz, D., & Ciardullo, R. 2015, *ApJL*, 804, L25, doi: [10.1088/2041-8205/804/1/L25](https://doi.org/10.1088/2041-8205/804/1/L25)
- Badenes, C., Maoz, D., & Draine, B. T. 2010, *MNRAS*, 407, 1301, doi: [10.1111/j.1365-2966.2010.17023.x](https://doi.org/10.1111/j.1365-2966.2010.17023.x)
- Barnbaum, C., & Morris, M. 1993, in *European Southern Observatory Conference and Workshop Proceedings*, Vol. 46, *European Southern Observatory Conference and Workshop Proceedings*, 280
- Beasor, E. R., Davies, B., Cabrera-Ziri, I., & Hurst, G. 2018, *MNRAS*, 479, 3101, doi: [10.1093/mnras/sty1744](https://doi.org/10.1093/mnras/sty1744)
- Benaglia, P., Romero, G. E., Koribalski, B., & Pollock, A. M. T. 2005, *A&A*, 440, 743, doi: [10.1051/0004-6361:20042617](https://doi.org/10.1051/0004-6361:20042617)
- Bernstein, R., Shtetman, S. A., Gunnels, S. M., Mochacki, S., & Athey, A. E. 2003, in *Society of Photo-Optical Instrumentation Engineers (SPIE) Conference Series*, Vol. 4841, *Instrument Design and Performance for Optical/Infrared Ground-based Telescopes*, ed. M. Iye & A. F. M. Moorwood, 1694–1704, doi: [10.1117/12.461502](https://doi.org/10.1117/12.461502)
- Biehle, G. T. 1994, *ApJ*, 420, 364, doi: [10.1086/173566](https://doi.org/10.1086/173566)
- Blaauw, A. 1961, *BAN*, 15, 265
- Boyer, M. L., McDonald, I., Srinivasan, S., et al. 2015, *ApJ*, 810, 116, doi: [10.1088/0004-637X/810/2/116](https://doi.org/10.1088/0004-637X/810/2/116)
- Boyer, M. L., Srinivasan, S., van Loon, J. T., et al. 2011, *AJ*, 142, 103, doi: [10.1088/0004-6256/142/4/103](https://doi.org/10.1088/0004-6256/142/4/103)
- Bozzetto, L. M., Filipović, M. D., Urošević, D., Kothes, R., & Crawford, E. J. 2014, *MNRAS*, 440, 3220, doi: [10.1093/mnras/stu499](https://doi.org/10.1093/mnras/stu499)
- Bozzetto, L. M., Filipović, M. D., Vukotić, B., et al. 2017, *ApJS*, 230, 2, doi: [10.3847/1538-4365/aa653c](https://doi.org/10.3847/1538-4365/aa653c)
- Calvet, N., & Hartmann, L. 1992, *ApJ*, 386, 239, doi: [10.1086/171010](https://doi.org/10.1086/171010)
- Cameron, A. G. W. 1955, *ApJ*, 121, 144, doi: [10.1086/145970](https://doi.org/10.1086/145970)
- Cameron, A. G. W., & Fowler, W. A. 1971, *ApJ*, 164, 111, doi: [10.1086/150821](https://doi.org/10.1086/150821)
- Cannon, R. C. 1993, *MNRAS*, 263, 817, doi: [10.1093/mnras/263.4.817](https://doi.org/10.1093/mnras/263.4.817)
- Cappa, C. E., & Herbstmeier, U. 2000, *AJ*, 120, 1963, doi: [10.1086/301556](https://doi.org/10.1086/301556)
- Chu, Y.-H., Chang, H.-W., Su, Y.-L., & Mac Low, M.-M. 1995, *ApJ*, 450, 157, doi: [10.1086/176127](https://doi.org/10.1086/176127)
- Ciotti, L., & D’Ercole, A. 1989, *A&A*, 215, 347
- Davies, B., Crowther, P. A., & Beasor, E. R. 2018, *MNRAS*, 478, 3138, doi: [10.1093/mnras/sty1302](https://doi.org/10.1093/mnras/sty1302)
- DeBoer, D. R., Gough, R. G., Bunton, J. D., et al. 2009, *IEEE Proceedings*, 97, 1507, doi: [10.1109/JPROC.2009.2016516](https://doi.org/10.1109/JPROC.2009.2016516)
- Díaz-Rodríguez, M., Murphy, J. W., Williams, B. F., Dalcanton, J. J., & Dolphin, A. E. 2021, arXiv e-prints, arXiv:2101.11012. <https://arxiv.org/abs/2101.11012>
- Dickel, J. R., McIntyre, V. J., Gruendl, R. A., & Milne, D. K. 2005, *AJ*, 129, 790, doi: [10.1086/426916](https://doi.org/10.1086/426916)
- Doherty, C. L., Gil-Pons, P., Lau, H. H. B., Lattanzio, J. C., & Siess, L. 2014a, *MNRAS*, 437, 195, doi: [10.1093/mnras/stt1877](https://doi.org/10.1093/mnras/stt1877)
- Doherty, C. L., Gil-Pons, P., Lau, H. H. B., et al. 2014b, *MNRAS*, 441, 582, doi: [10.1093/mnras/stu571](https://doi.org/10.1093/mnras/stu571)
- Doherty, C. L., Gil-Pons, P., Siess, L., & Lattanzio, J. C. 2017, *PASA*, 34, e056, doi: [10.1017/pasa.2017.52](https://doi.org/10.1017/pasa.2017.52)
- Doherty, C. L., Gil-Pons, P., Siess, L., Lattanzio, J. C., & Lau, H. H. B. 2015, *MNRAS*, 446, 2599, doi: [10.1093/mnras/stu2180](https://doi.org/10.1093/mnras/stu2180)
- Dorigo Jones, J., Oey, M. S., Paggeot, K., Castro, N., & Moe, M. 2020, *ApJ*, 903, 43, doi: [10.3847/1538-4357/abbc6b](https://doi.org/10.3847/1538-4357/abbc6b)
- Draine, B. T. 2011, *Physics of the Interstellar and Intergalactic Medium* (Princeton University Press)
- Eldridge, J. J., Langer, N., & Tout, C. A. 2011, *MNRAS*, 414, 3501, doi: [10.1111/j.1365-2966.2011.18650.x](https://doi.org/10.1111/j.1365-2966.2011.18650.x)

- European Organization For Nuclear Research, & OpenAIRE. 2013, Zenodo, CERN, doi: [10.25495/7GXK-RD71](https://doi.org/10.25495/7GXK-RD71)
- Filipović, M. D., Bohlsen, T., Reid, W., et al. 2002, MNRAS, 335, 1085, doi: [10.1046/j.1365-8711.2002.05702.x](https://doi.org/10.1046/j.1365-8711.2002.05702.x)
- Filipović, M. D., Payne, J. L., Reid, W., et al. 2005, MNRAS, 364, 217, doi: [10.1111/j.1365-2966.2005.09554.x](https://doi.org/10.1111/j.1365-2966.2005.09554.x)
- Frail, D. A., Goss, W. M., & Whiteoak, J. B. Z. 1994, ApJ, 437, 781, doi: [10.1086/175038](https://doi.org/10.1086/175038)
- Gaensler, B. M., McClure-Griffiths, N. M., Oey, M. S., et al. 2005, ApJL, 620, L95, doi: [10.1086/428725](https://doi.org/10.1086/428725)
- Gaia Collaboration, Brown, A. G. A., Vallenari, A., et al. 2018a, ArXiv e-prints, arXiv:1804.09365. <https://arxiv.org/abs/1804.09365>
- . 2020, arXiv e-prints, arXiv:2012.01533. <https://arxiv.org/abs/2012.01533>
- Gaia Collaboration, Helmi, A., van Leeuwen, F., et al. 2018b, A&A, 616, A12, doi: [10.1051/0004-6361/201832698](https://doi.org/10.1051/0004-6361/201832698)
- Gandhi, P., Buckley, D. A. H., Charles, P., et al. 2020, arXiv e-prints, arXiv:2009.07277. <https://arxiv.org/abs/2009.07277>
- Garcia-Berro, E., & Iben, I. 1994, ApJ, 434, 306, doi: [10.1086/174729](https://doi.org/10.1086/174729)
- García-Hernández, D. A., García-Lario, P., Plez, B., et al. 2006, Science, 314, 1751, doi: [10.1126/science.1133706](https://doi.org/10.1126/science.1133706)
- . 2007, A&A, 462, 711, doi: [10.1051/0004-6361:20065785](https://doi.org/10.1051/0004-6361:20065785)
- García-Hernández, D. A., Zamora, O., Yagüe, A., et al. 2013, A&A, 555, L3, doi: [10.1051/0004-6361/201321818](https://doi.org/10.1051/0004-6361/201321818)
- Gervais, S., & St-Louis, N. 1999, AJ, 118, 2394, doi: [10.1086/301065](https://doi.org/10.1086/301065)
- Gillet, D., Maurice, E., Bouchet, P., & Ferlet, R. 1985, A&A, 148, 155
- Girardi, L., Bressan, A., Bertelli, G., & Chiosi, C. 2000, A&AS, 141, 371, doi: [10.1051/aas:2000126](https://doi.org/10.1051/aas:2000126)
- Graczyk, D., Pietrzyński, G., Thompson, I. B., et al. 2014, ApJ, 780, 59, doi: [10.1088/0004-637X/780/1/59](https://doi.org/10.1088/0004-637X/780/1/59)
- Gustafsson, B., Edvardsson, B., Eriksson, K., et al. 2008, A&A, 486, 951, doi: [10.1051/0004-6361:200809724](https://doi.org/10.1051/0004-6361:200809724)
- Haberl, F., & Sturm, R. 2016, A&A, 586, A81, doi: [10.1051/0004-6361/201527326](https://doi.org/10.1051/0004-6361/201527326)
- Harris, J., & Zaritsky, D. 2004, AJ, 127, 1531, doi: [10.1086/381953](https://doi.org/10.1086/381953)
- . 2009, AJ, 138, 1243, doi: [10.1088/0004-6256/138/5/1243](https://doi.org/10.1088/0004-6256/138/5/1243)
- Hartmann, L., Hewett, R., & Calvet, N. 1994, ApJ, 426, 669, doi: [10.1086/174104](https://doi.org/10.1086/174104)
- Harvey-Smith, L., Chapman, J., Lenc, E., et al. 2016, ASKAP Data Products for Project AS033 (ASKAP Science Commissioning): images and visibilities. <http://hdl.handle.net/102.100.100/40062?index=1>
- Herbig, G. H., & Soderblom, D. R. 1982, ApJ, 252, 610, doi: [10.1086/159588](https://doi.org/10.1086/159588)
- Höfner, S., & Olofsson, H. 2018, A&A Rv, 26, 1, doi: [10.1007/s00159-017-0106-5](https://doi.org/10.1007/s00159-017-0106-5)
- Husser, T. O., Wende-von Berg, S., Dreizler, S., et al. 2013, A&A, 553, A6, doi: [10.1051/0004-6361/201219058](https://doi.org/10.1051/0004-6361/201219058)
- Jones, S., Ritter, C., Herwig, F., et al. 2016, MNRAS, 455, 3848, doi: [10.1093/mnras/stv2488](https://doi.org/10.1093/mnras/stv2488)
- Jones, S., Hirschi, R., Nomoto, K., et al. 2013, ApJ, 772, 150, doi: [10.1088/0004-637X/772/2/150](https://doi.org/10.1088/0004-637X/772/2/150)
- Joseph, T. D., Filipović, M. D., Crawford, E. J., et al. 2019, MNRAS, 490, 1202, doi: [10.1093/mnras/stz2650](https://doi.org/10.1093/mnras/stz2650)
- Karakas, A. I., García-Hernández, D. A., & Lugaro, M. 2012, ApJ, 751, 8, doi: [10.1088/0004-637X/751/1/8](https://doi.org/10.1088/0004-637X/751/1/8)
- Karakas, A. I., & Lattanzio, J. C. 2014, PASA, 31, e030, doi: [10.1017/pasa.2014.21](https://doi.org/10.1017/pasa.2014.21)
- Karakas, A. I., & Lugaro, M. 2016, ApJ, 825, 26, doi: [10.3847/0004-637X/825/1/26](https://doi.org/10.3847/0004-637X/825/1/26)
- Karakas, A. I., Lugaro, M., Carlos, M., et al. 2018, MNRAS, 477, 421, doi: [10.1093/mnras/sty625](https://doi.org/10.1093/mnras/sty625)
- Kelson, D. D. 2003, PASP, 115, 688, doi: [10.1086/375502](https://doi.org/10.1086/375502)
- Kelson, D. D., Illingworth, G. D., van Dokkum, P. G., & Franx, M. 2000, ApJ, 531, 159, doi: [10.1086/308445](https://doi.org/10.1086/308445)
- Kim, S., Staveley-Smith, L., Dopita, M. A., et al. 2003, ApJS, 148, 473, doi: [10.1086/376980](https://doi.org/10.1086/376980)
- Kochanek, C. S. 2022, MNRAS, 511, 3428, doi: [10.1093/mnras/stac098](https://doi.org/10.1093/mnras/stac098)
- Kramida, A., Yu. Ralchenko, Reader, J., & and NIST ASD Team. 2021, NIST Atomic Spectra Database (ver. 5.9), [Online]. Available: <https://physics.nist.gov/asd> [2021, December 2]. National Institute of Standards and Technology, Gaithersburg, MD.
- Krtićka, J. 2014, A&A, 564, A70, doi: [10.1051/0004-6361/201321980](https://doi.org/10.1051/0004-6361/201321980)
- Kuchner, M. J., Vakil, D., Smith, V. V., et al. 2002, in Stellar Collisions, Mergers and their Consequences, Vol. 263, 131
- Kudashkina, L. S., & Rudnitskij, G. M. 1994, Odessa Astronomical Publications, 7, 66
- Lau, H. H. B., Doherty, C. L., Gil-Pons, P., & Lattanzio, J. C. 2011, in Astronomical Society of the Pacific Conference Series, Vol. 445, Why Galaxies Care about AGB Stars II: Shining Examples and Common Inhabitants, ed. F. Kerschbaum, T. Lebzelter, & R. F. Wing, 45

- Leavitt, H. S. 1984, 1777 variables in the Magellanic clouds. (Annals of Harvard College Observatory). https://cosmology.education/documents/cepheides_leavitt.pdf
- Lennon, D. J., Evans, C. J., van der Marel, R. P., et al. 2018, *A&A*, 619, A78, doi: [10.1051/0004-6361/201833465](https://doi.org/10.1051/0004-6361/201833465)
- Leonard, P. J. T., Hills, J. G., & Dewey, R. J. 1994, *ApJL*, 423, L19, doi: [10.1086/187225](https://doi.org/10.1086/187225)
- Levesque, E. M., Massey, P., Olsen, K. A. G., et al. 2005, *ApJ*, 628, 973, doi: [10.1086/430901](https://doi.org/10.1086/430901)
- Levesque, E. M., Massey, P., Żytkow, A. N., & Morrell, N. 2014, *MNRAS*, 443, L94, doi: [10.1093/mnrasl/slu080](https://doi.org/10.1093/mnrasl/slu080)
- Lindgren, L., Lammers, U., Hobbs, D., et al. 2012, *A&A*, 538, A78, doi: [10.1051/0004-6361/201117905](https://doi.org/10.1051/0004-6361/201117905)
- Lindgren, L., Hernández, J., Bombrun, A., et al. 2018, *A&A*, 616, A2, doi: [10.1051/0004-6361/201832727](https://doi.org/10.1051/0004-6361/201832727)
- Liu, X. W., Xu, R. X., van den Heuvel, E. P. J., et al. 2015, *ApJ*, 799, 233, doi: [10.1088/0004-637X/799/2/233](https://doi.org/10.1088/0004-637X/799/2/233)
- Maggi, P., Haberl, F., Kavanagh, P. J., et al. 2016, *A&A*, 585, A162, doi: [10.1051/0004-6361/201526932](https://doi.org/10.1051/0004-6361/201526932)
- Maggi, P., Filipović, M. D., Vukotić, B., et al. 2019, *A&A*, 631, A127, doi: [10.1051/0004-6361/201936583](https://doi.org/10.1051/0004-6361/201936583)
- Maao, D., & Badenes, C. 2010, *MNRAS*, 407, 1314, doi: [10.1111/j.1365-2966.2010.16988.x](https://doi.org/10.1111/j.1365-2966.2010.16988.x)
- Massey, P., Neugent, K. F., Dorn-Wallenstein, T. Z., et al. 2021, *ApJ*, 922, 177, doi: [10.3847/1538-4357/ac15f5](https://doi.org/10.3847/1538-4357/ac15f5)
- Massey, P., & Olsen, K. A. G. 2003, *AJ*, 126, 2867, doi: [10.1086/379558](https://doi.org/10.1086/379558)
- Mathewson, D. S., & Clarke, J. N. 1973, *ApJ*, 180, 725, doi: [10.1086/152002](https://doi.org/10.1086/152002)
- Mazzitelli, I., D’Antona, F., & Ventura, P. 1999, *A&A*, 348, 846. <https://arxiv.org/abs/astro-ph/9907245>
- McClure-Griffiths, N. M., Dickey, J. M., Gaensler, B. M., & Green, A. J. 2001, *ApJ*, 562, 424, doi: [10.1086/323859](https://doi.org/10.1086/323859)
- McClure-Griffiths, N. M., Dénes, H., Dickey, J. M., et al. 2018, *Nature Astronomy*, 2, 901, doi: [10.1038/s41550-018-0608-8](https://doi.org/10.1038/s41550-018-0608-8)
- Miyaji, S., Nomoto, K., Yokoi, K., & Sugimoto, D. 1980, *PASJ*, 32, 303
- Mujres, L. E., Vink, J. S., de Koter, A., Müller, P. E., & Langer, N. 2012, *A&A*, 537, A37, doi: [10.1051/0004-6361/201015818](https://doi.org/10.1051/0004-6361/201015818)
- Neugent, K. F., Levesque, E. M., Massey, P., Morrell, N. I., & Drout, M. R. 2020, *ApJ*, 900, 118, doi: [10.3847/1538-4357/ababaa](https://doi.org/10.3847/1538-4357/ababaa)
- Neugent, K. F., Massey, P., Skiff, B., et al. 2010, *ApJ*, 719, 1784, doi: [10.1088/0004-637X/719/2/1784](https://doi.org/10.1088/0004-637X/719/2/1784)
- Neugent, K. F., Massey, P., Skiff, B., & Meynet, G. 2012, *ApJ*, 749, 177, doi: [10.1088/0004-637X/749/2/177](https://doi.org/10.1088/0004-637X/749/2/177)
- Oey, M. S., Dorigo Jones, J., Castro, N., et al. 2018, *ApJL*, 867, L8, doi: [10.3847/2041-8213/aae892](https://doi.org/10.3847/2041-8213/aae892)
- O’Grady, A. J. G., Drout, M. R., Shappee, B. J., et al. 2020, *ApJ*, 901, 135, doi: [10.3847/1538-4357/abafad](https://doi.org/10.3847/1538-4357/abafad)
- Paxton, B., Bildsten, L., Dotter, A., et al. 2011, *ApJS*, 192, 3, doi: [10.1088/0067-0049/192/1/3](https://doi.org/10.1088/0067-0049/192/1/3)
- Paxton, B., Marchant, P., Schwab, J., et al. 2015, *ApJS*, 220, 15, doi: [10.1088/0067-0049/220/1/15](https://doi.org/10.1088/0067-0049/220/1/15)
- Paxton, B., Schwab, J., Bauer, E. B., et al. 2018, *ApJS*, 234, 34, doi: [10.3847/1538-4365/aaa5a8](https://doi.org/10.3847/1538-4365/aaa5a8)
- Paxton, B., Smolec, R., Schwab, J., et al. 2019, arXiv e-prints, arXiv:1903.01426. <https://arxiv.org/abs/1903.01426>
- Payne-Gaposchkin, C., & Gaposchkin, S. 1966, *Smithsonian Contributions to Astrophysics*, 9, 1
- Pietrzyński, G., Graczyk, D., Gieren, W., et al. 2013, *Nature*, 495, 76, doi: [10.1038/nature11878](https://doi.org/10.1038/nature11878)
- Podsiadlowski, P., Cannon, R. C., & Rees, M. J. 1995, *MNRAS*, 274, 485, doi: [10.1093/mnras/274.2.485](https://doi.org/10.1093/mnras/274.2.485)
- Poelarends, A. J. T., Herwig, F., Langer, N., & Heger, A. 2008, *ApJ*, 675, 614, doi: [10.1086/520872](https://doi.org/10.1086/520872)
- Ramírez-Ballinas, I., Reyes-Iturbide, J., Toalá, J. A., & Rosado, M. 2019, *ApJ*, 885, 116, doi: [10.3847/1538-4357/ab44cf](https://doi.org/10.3847/1538-4357/ab44cf)
- Renzo, M., Zapartas, E., de Mink, S. E., et al. 2019, *A&A*, 624, A66, doi: [10.1051/0004-6361/201833297](https://doi.org/10.1051/0004-6361/201833297)
- Richter, H., & Wood, P. R. 2001, *A&A*, 369, 1027, doi: [10.1051/0004-6361:20010156](https://doi.org/10.1051/0004-6361:20010156)
- Ritossa, C., García-Berro, E., & Iben, Icko, J. 1999, *ApJ*, 515, 381, doi: [10.1086/307017](https://doi.org/10.1086/307017)
- Ritter, C., Herwig, F., Jones, S., et al. 2018, *MNRAS*, 480, 538, doi: [10.1093/mnras/sty1729](https://doi.org/10.1093/mnras/sty1729)
- Sackmann, I. J., & Boothroyd, A. I. 1992, *ApJL*, 392, L71, doi: [10.1086/186428](https://doi.org/10.1086/186428)
- Sarbadhicary, S. K., Heiger, M., Badenes, C., et al. 2021, *ApJ*, 912, 140, doi: [10.3847/1538-4357/abca86](https://doi.org/10.3847/1538-4357/abca86)
- Siess, L. 2010, *A&A*, 512, A10, doi: [10.1051/0004-6361/200913556](https://doi.org/10.1051/0004-6361/200913556)
- Smith, V. V., Plez, B., Lambert, D. L., & Lubowich, D. A. 1995, *ApJ*, 441, 735, doi: [10.1086/175395](https://doi.org/10.1086/175395)
- Soszyński, I., Udalski, A., Szymański, M. K., et al. 2015, *AcA*, 65, 297. <https://arxiv.org/abs/1601.01318>
- . 2016, *AcA*, 66, 131. <https://arxiv.org/abs/1606.02727>
- . 2017, *AcA*, 67, 103, doi: [10.32023/0001-5237/67.2.1](https://doi.org/10.32023/0001-5237/67.2.1)
- Taam, R. E., Bodenheimer, P., & Ostriker, J. P. 1978, *ApJ*, 222, 269, doi: [10.1086/156142](https://doi.org/10.1086/156142)
- Tabernero, H. M., Dorda, R., Negueruela, I., & Marfil, E. 2021, *A&A*, 646, A98, doi: [10.1051/0004-6361/202039236](https://doi.org/10.1051/0004-6361/202039236)
- Taylor, M. B. 2005, in *Astronomical Society of the Pacific Conference Series*, Vol. 347, *Astronomical Data Analysis Software and Systems XIV*, ed. P. Shopbell, M. Britton, & R. Ebert, 29

- Thorne, K. S., & Żytkow, A. N. 1975, *ApJL*, 199, L19, doi: [10.1086/181839](https://doi.org/10.1086/181839)
- . 1977, *ApJ*, 212, 832, doi: [10.1086/155109](https://doi.org/10.1086/155109)
- Tody, D. 1986, in *Society of Photo-Optical Instrumentation Engineers (SPIE) Conference Series*, Vol. 627, Proc. SPIE, ed. D. L. Crawford, 733, doi: [10.1117/12.968154](https://doi.org/10.1117/12.968154)
- Tody, D. 1993, in *Astronomical Society of the Pacific Conference Series*, Vol. 52, *Astronomical Data Analysis Software and Systems II*, ed. R. J. Hanisch, R. J. V. Brissenden, & J. Barnes, 173
- Tout, C. A., Żytkow, A. N., Church, R. P., et al. 2014, *MNRAS*, 445, L36, doi: [10.1093/mnrasl/slu131](https://doi.org/10.1093/mnrasl/slu131)
- Townsend, R. H. D., & Teitler, S. A. 2013, *MNRAS*, 435, 3406, doi: [10.1093/mnras/stt1533](https://doi.org/10.1093/mnras/stt1533)
- van den Heuvel, E. P. J., Portegies Zwart, S. F., Bhattacharya, D., & Kaper, L. 2000, *A&A*, 364, 563. <https://arxiv.org/abs/astro-ph/0005245>
- van der Heyden, K. J., Bleeker, J. A. M., & Kaastra, J. S. 2004, *A&A*, 421, 1031, doi: [10.1051/0004-6361:20034156](https://doi.org/10.1051/0004-6361:20034156)
- van Hoof, P. A. M. 2018, *Galaxies*, 6, 63, doi: [10.3390/galaxies6020063](https://doi.org/10.3390/galaxies6020063)
- van Loon, J. T., Cioni, M. R. L., Zijlstra, A. A., & Loup, C. 2005, *A&A*, 438, 273, doi: [10.1051/0004-6361:20042555](https://doi.org/10.1051/0004-6361:20042555)
- van Raai, M. A., Lugaro, M., Karakas, A. I., García-Hernández, D. A., & Yong, D. 2012, *A&A*, 540, A44, doi: [10.1051/0004-6361/201117896](https://doi.org/10.1051/0004-6361/201117896)
- Vanture, A. D., Zucker, D., & Wallerstein, G. 1999, *ApJ*, 514, 932, doi: [10.1086/306956](https://doi.org/10.1086/306956)
- Vassiliadis, E., & Wood, P. R. 1993, *ApJ*, 413, 641, doi: [10.1086/173033](https://doi.org/10.1086/173033)
- Ventura, P., D'Antona, F., Di Criscienzo, M., et al. 2012, *ApJL*, 761, L30, doi: [10.1088/2041-8205/761/2/L30](https://doi.org/10.1088/2041-8205/761/2/L30)
- Walborn, N. R., Gamen, R. C., Morrell, N. I., et al. 2017, *AJ*, 154, 15, doi: [10.3847/1538-3881/aa6195](https://doi.org/10.3847/1538-3881/aa6195)
- Walker, M. F. 1972, *ApJ*, 175, 89, doi: [10.1086/151540](https://doi.org/10.1086/151540)
- Weaver, R., McCray, R., Castor, J., Shapiro, P., & Moore, R. 1977, *ApJ*, 218, 377, doi: [10.1086/155692](https://doi.org/10.1086/155692)
- Williams, B. F., Hillis, T. J., Murphy, J. W., et al. 2018, *ApJ*, 860, 39, doi: [10.3847/1538-4357/aaba7d](https://doi.org/10.3847/1538-4357/aaba7d)
- Williams, R. M., Chu, Y.-H., Dickel, J. R., et al. 1999, *ApJS*, 123, 467, doi: [10.1086/313246](https://doi.org/10.1086/313246)
- Wolf, B., & Stahl, O. 1990, *A&A*, 235, 340
- Yanchulova Merica-Jones, P., Sandstrom, K. M., Johnson, L. C., et al. 2017, *ApJ*, 847, 102, doi: [10.3847/1538-4357/aa8a67](https://doi.org/10.3847/1538-4357/aa8a67)
- Yang, M., & Jiang, B. W. 2011, *ApJ*, 727, 53, doi: [10.1088/0004-637X/727/1/53](https://doi.org/10.1088/0004-637X/727/1/53)
- . 2012, *ApJ*, 754, 35, doi: [10.1088/0004-637X/754/1/35](https://doi.org/10.1088/0004-637X/754/1/35)
- Zaritsky, D., Harris, J., Thompson, I. B., & Grebel, E. K. 2004, *AJ*, 128, 1606, doi: [10.1086/423910](https://doi.org/10.1086/423910)
- Zaritsky, D., Harris, J., Thompson, I. B., Grebel, E. K., & Massey, P. 2002, *AJ*, 123, 855, doi: [10.1086/338437](https://doi.org/10.1086/338437)